Max-Planck-Institut
für Meteorologie

REPORT No. 228

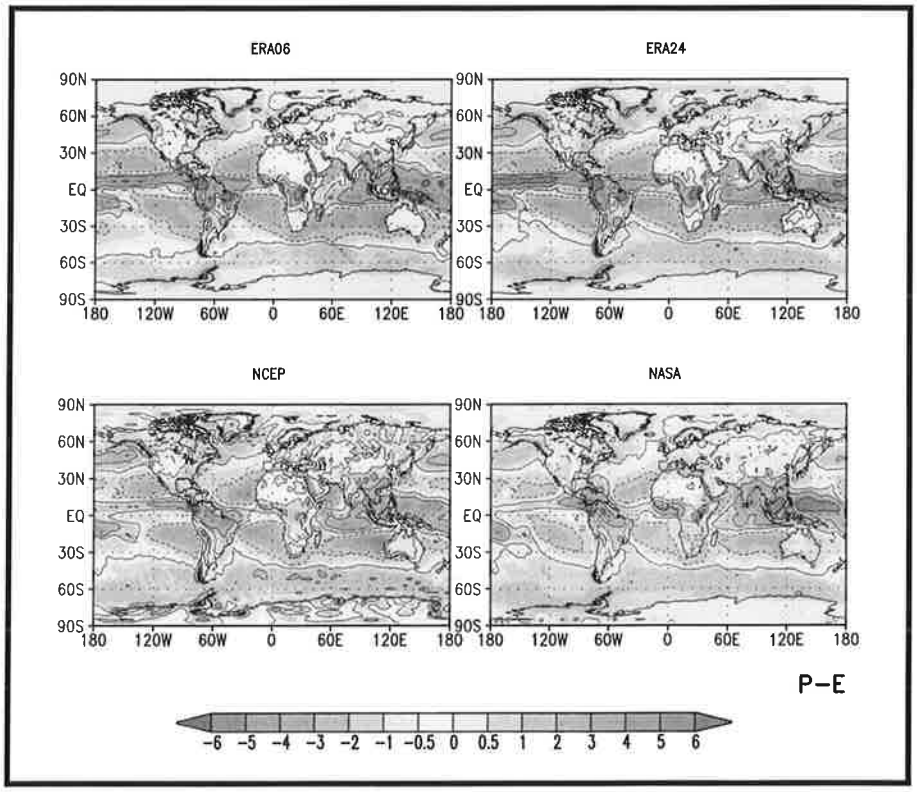

EVALUATION OF THE HYDROLOGICAL CYCLE IN REANALYSES AND OBSERVATIONS

by

Martin Stendel • Klaus Arpe

HAMBURG, February 1997

AUTHORS:

Martin Stendel,
Klaus Arpe

Max-Planck-Institut für Meteorologie
Hamburg
F. R. Germany

MAX-PLANCK-INSTITUT
FÜR METEOROLOGIE
BUNDESSTRASSE 55
D-20146 HAMBURG
F.R. GERMANY

Tel.: +49 - (0)40 - 411 73 - 0
Telefax: +49 - (0)40 - 411 73 - 298
E-Mail: <name>@dkrz.de

Evaluation of the Hydrological Cycle in Reanalyses and Observations

Martin Stendel and Klaus Arpe

Max-Planck-Institut für Meteorologie, Hamburg, Germany

ISSN 0937 - 1060

Abstract

An evaluation of the components of the hydrological cycle in the reanalyses from the ECMWF has been performed. These are compared to the reanalyses from NCEP and NASA as well as analyses and observations from different data sources and several satellite estimates.

With respect to GPCP precipitation data, the ECMWF reanalyses are superior to the reanalyses from NCEP and NASA in the extratropics. No clear decision can be made in the tropics where all reanalyses overestimate precipitation. The NASA reanalysis does not catch correctly the annual cycle of tropical precipitation. There are some problematic regions in the ECMWF reanalysis, including the Andes, where too much precipitation is analyzed, and the Alps and Antarctica which are too dry.

There is a 10^{o} southward shift of the ITCZ over Africa in the ECMWF reanalysis around 1987. A probably non-meteorological long term trend is visible in the tropics with a slight increase of oceanic precipitation and a decrease of latent heat flux. The reason for this is not clear. Therefore there are applications for which the NCEP reanalyses may be more suitable.

The quality of the hydrological cycle has been appraised by long-term means of the difference of precipitation and evaporation (P-E) and a comparison to observed river discharge. None of the reanalyses has a closed hydrological budget over subtropical land points. The 12-24 hour forecast of ECMWF performs best in this respect.

The ECMWF reanalysis shows a clear spinup of about 15% nearly everywhere. On the whole, especially in winter over land, the 12 to 24 hour forecasts fit the observations best and give the most consistent picture. A positive effect on the construction of global precipitation datasets (as filling data sparse areas in the GPCP analyses) is likely.

Hadley cell due to the introduction of diabatic Normal Mode Initialization (NMI) in 1982, changes in model resolution (1983, 1985) and in the analysis scheme (1986, 1989) are clearly visible. Arpe (1990) and Trenberth (1992) have discussed these impacts from model changes in detail. Schneider et al. (1992) have compared area averages of precipitation from the then operational forecasts of the ECMWF with conventional measurements and found a strong sensitivity to model changes, with relative errors of up to 100% without a clear seasonal signature. Due to these obvious deficiencies, it has been suggested (Bengtsson and Shukla, 1988) to "re-analyze" global atmospheric datasets with a frozen data assimilation scheme. At the ECMWF, such a reanalysis project has been completed for the period 1979 to 1993, referred to as ERA in the remainder of this text. Reanalyses have recently also been carried out at the National Centers for Environmental Prediction[2] / National Center for Atmospheric Research (hereafter denoted NCEP) and at the Data Assimilation Office of NASA's Goddard Space Flight Center (hereafter denoted NASA). Documentation of these reanalysis datasets and assimilation systems can be found in Kalnay et al. (1995) for the former project and in Schubert et al. (1993) for the latter one.

This study aims to evaluate the realism of the precipitation estimates by the European Centre for Medium-Range Weather Forecasts (ECMWF) reanalysis. A comparison of different analysis schemes can help to identify sensitive areas, and in regions with a good observational data coverage one can compare the estimated precipitation with observations. Also the degree of adjustment between the analysis and the short-range forecasts (generally referred to as spinup) gives some measure of the quality of the analysis data. The results are only indicative, and further investigations are in progress.

The paper is organized as follows: In section 2, a short description of the datasets that are used for the validation is given. Section 3 deals with long-term global precipitation distributions. In sections 4 and 5, the variability of precipitation on different time scales, from interannual to interdiurnal, are investigated. In section 6, a detailed discussion of the spinup follows. The other components of the hydrological cycle are addressed in sections 7 (evaporation) and 8 (river runoff). The results are discussed in section 9, which is followed by conclusions and some final remarks.

---

[2] Formerly National Meteorological Center (NMC).

Another possibility of satellite rainfall estimation is the use of microwave measurements from the Special Sensor Microwave Imager (SSM/I) on board of polar orbiting satellites. Radiances are measured at four frequencies near 19, 22, 37 and 85 GHz, respectively. At these frequencies, not only the microwave emission of hydrometeors can be detected, but also their effect on radiative transfer due to absorption and scattering. Since land surfaces have nearly the same emissivity as water clouds, SSM/I precipitation estimates based on emission are meaningful only over the oceans. An algorithm from Wilheit et al. (1991) is applied that assumes a log-normal precipitation histogram and estimates the freezing level from the 19 GHz and 22 GHz channels. Precipitation estimates based on the scattering by hydrometeors are applicable also over land. Here algorithms from Grody (1991) and Weng and Grody (1994) are applied. The SSM/I is a multi-channel instrument and therefore allows the retrieval of a variety of parameters, including sea ice and snow cover and, at 85 GHz, water vapour, liquid water and rain. The latter frequency provides a plain relation between precipitation rate and brightness temperature, the main effect being the scattering in ice clouds (Adler et al., 1991). However, due to the sun-synchronous satellite orbit, at the best only two SSM/I soundings per day are available for a given point so that the diurnal cycle cannot be determined except for periods when observations from more than one satellite are available (Chang et al., 1995). When comparing monthly means as in this paper, it has to be considered that GPI and SSM/I emission data are potentially biased since they are based on pentad averages that do not exactly coincide with calendar months.

From the Microwave Sounding Unit (MSU) that is primarily used to estimate the vertical temperature distribution (Grody, 1983), the liquid water content of the atmosphere can be calculated (Spencer, 1993). Monthly precipitation sums are then obtained via an empirical relation.

Both infrared and SSM/I methods are not applicable in the polar regions, so that there are several gridpoints in high latitudes where neither gauge nor satellite observations exist. If it is essential to have global datasets, as in GPCP, it is necessary to take into account the results of numerical models. There are, however, a number of caveats. The physical process of the formation of precipitation has to be parameterized and may depend on the horizontal and vertical resolution of contemporary global models. The horizontal resolution is also responsible for the heavily smoothed representation of terrain that may influence the representation of e.g. orographically forced rain. Observed precipitation data does not enter into the initialization of most models (for an exception see Krishnamurti et al., 1991). Furthermore, the three-dimensional distribution of cloud water and rain water is quantitatively unknown. Furthermore, due to imbalances in the initial fields, a "spinup" of precipitation occurs.

The NCEP reanalysis was performed with the NCEP Medium Range Forecast (MRF) model and the operational Spectral Statistical Interpolation (SSI) procedure (Parrish and Derber, 1992; Kalnay et al., 1993). A T62 spectral resolution with 28 sigma levels, seven of them below 850 hPa, is used. We had available the period 1982-1993. The lower boundary is given by mean orographic height. Convective parameterization is performed by a simplified Arakawa-Schubert convective scheme (Pan and Wu, 1994). The NCEP reanalyses need not be initialized because the statistical spectral interpolation eliminates imbalances in the initial state. Soil moisture is obtained from the two-layer implicit scheme of Pan and Mahrt (1987).

NASA took a different approach for the assimilation of observational data: a continuous assimilation is used, where analysis increments are used as constant forcings throughout the integration between two analysis steps. Therefore no initialization is necessary (Bloom et al., 1995). The reanalysis is carried out using a grid point model. It is performed with the Goddard Earth Observing System (GEOS) GCM (Takacs et al., 1994) and an optimum interpolation scheme (Pfaendtner et al., 1995) on a horizontal grid of 2.5° longitude by 2° latitude with 20 vertical sigma levels, four of them below 850 hPa. NASA data are available for 1985 to 1993. The model uses an relaxed Arakawa-Schubert parameterization (Moorthi and Suarez, 1992) that is a simplification of the original Arakawa-Schubert (1974) scheme. Soil moisture is computed off-line based on a bucket model that incorporates monthly means of surface air temperature and precipitation (Higgins et al., 1996).

There are also differences in the SST and sea ice cover datasets used that might impact the atmosphere. In the ECMWF reanalysis, the following were used: 1° monthly analyses from the UK Meteorological Officce (GISST) for December 1978 and January 1980 to October 1981 and 1° weekly optimum-interpolated SST analyses of Reynolds and Smith (1994) for November 1981 to the end of the period. Special arrangements were made with NCEP and NASA to enable each reanalysis to use an idential set of SSTs and sea ice limits for 1979, namely the EOF-enhanced SST from the combined UK Meteorological Office (GISST) and NCEP dataset. Sea ice limits from SMMR and SSM/I are inserted through a post-analysis procedure (Nomura, 1995). While NCEP uses the improved global optimum interpolated (OI) SST analyses of Reynolds and Smith (1994), NASA incorporates the blended SST analyses of Reynolds (1988) and Reynolds and Marsico (1993). Differences between OI and blended analyses can be expected in regions of high SST gradients, e.g. the East Pacific (Reynolds and Smith, 1994) and near ice edges. After July 1987, SSM/I satellite winds are included in the NCEP, but neither in the ECMWF nor NASA reanalysis.

ispheres. Over the Indian subcontinent, the reanalyses result in wetter conditions at the west coast of India, with drier than observed conditions away from the coast. Here the interpolation from a resolution of 2.5^{o} in GPCP to a N80 resolution used in ERA may have an effect.

The zonal means of the reanalyses in Fig. 2 show the secondary precipitation maxima in the temperate latitudes displaced poleward, especially on the Southern Hemisphere. There is a general tendency to underestimate land precipitation in boreal winter in the reanalyses (Fig. 3a) and overestimate it in summer (Fig. 3b). In detail, the NCEP reanalysis shows excessive summer precipitation over Europe (Table 1), and both NCEP and especially NASA reanalyses are much too wet over large parts of North America in summer (Fig. 4), which is connected to excessive evaporation (Stendel and Arpe, 1996). The wet bias in ERA is much smaller. On the other hand, in NH winter, NCEP and NASA exhibit a dry bias in the extratropics, as compared to various observational datasets and to the Legates and Willmott climatology (see also Molod et al., 1995). Good agreement is found between observations and ECMWF reanalyses, with differences less than 0.2 mm/day (about 10%) in large parts of North America and Asia. However, a dry bias can be noticed for ERA over Europe, ERA24 being slightly superior in this respect to the first guesses (compare Fig. 3a). Over mid-latitude oceans generally less precipitation is found in the reanalyses than in GPCP.

Of special interest is the area parallel to the North American coast along the Atlantic cyclone track (Fig. 4). The GPCP analysis consists here of estimates using SSM/I observations. It would be extremely interesting to know if the models of both analysis schemes have the same systematic error of generating too little precipitation in young developing cyclones or if the estimates by SSM/I suffer from an overestimation in these young cyclones. Probably the algorithms for the estimation of precipitation from SSM/I observations need to be different in case of young and of fully developed cyclones. In the Precipitation Intercomparison Project (PIP-3), all SSM/I estimates show similar high values in this area with the only exception of the Bristol University algorithm which was tuned with midlatitude observations.

The NCEP reanalysis shows unrealistic noise in the polar regions. This is not due to the Gibbs phenomenon as previously thought, but rather to the poor approximation of horizontal moisture diffusion in the boundary layer when transforming from σ to pressure coordinates. Unrealistic corrections are applied in high latitudes and elevations, leading to the spurious precipitation visible in Fig. 3a and 3b. An a-posteriori correction has recently been developed (NCEP Reanalysis Problem Report, 1996), but the corrected precipitation

Whereas, by and large, the precipitation estimates over land agree well, there is a considerable degree of uncertainty in ocean precipitation rates. Since there are virtually no direct observations, the GPCP dataset has to rely on the GPI and SSM/I estimates. In Fig. 2, all datasets show a primary maximum of precipitation near 5°N and secondary maxima between 15°S (in DJF) and 10°S (in JJA), and there is a wet bias between 25°S and 25°N, as compared to GPCP estimates. This bias is larger in DJF than in JJA and also larger in ERA than in NCEP. Over the Western Pacific (Fig. 3), the SPCZ has a more E-W orientation in the reanalyses than in the GPCP analysis, and this deficiency is stronger in the NCEP than in the ERA data. None of the datasets supports the relative precipitation maximum at 60°S in the Legates and Willmott (1990) climatology (not shown here). It therefore appears highly unrealistic (cf. Roeckner et al., 1992).

The precipitation over the polar caps is hardly known since almost no operational observations of precipitation are available. In Fig. 5, we use the annual cycle at the Antarctic station Vostok (78°27'S, 106°52'E, data from Genthon and Braun, 1995) and at the Russian North Polar ice drift stations (data from Radionov, to be published). For the Arctic these observations agree with the values by ERA and Legates, while NCEP provides an overestimate in summer. At Vostok the ERA values are too low during southern winter while the Legates and Willmott data give by far higher values. Due to the high spatial variability in the NCEP precipitation data in polar regions that was mentioned above, the NCEP values depend strongly on the choice of the averaging region.

A point of concern is the relation between stratiform and convective precipitation, since the underlying physical processes are different. In the reanalyses from ECMWF and NCEP, the total precipitation is separated into both precipitation types, but not in the NASA reanalysis data available to us. Large scale precipitation is typically connected to extratropical baroclinic waves. However, a significant proportion of tropical precipitation also is of stratiform nature and falls from anvils of cumulonimbus clouds, as indicated by observations during GATE. In the ECMWF reanalysis such a horizontal distribution is visible (not shown), with maximum values of stratiform precipitation over the cyclone track regions of the respective winter hemisphere and in the ITCZ. In summer, the Indian summer monsoon is also clearly visible. In contrast to the ECMWF reanalyses, there is virtually no tropical large scale precipitation in the NCEP reanalyses except at isolated grid points over the highlands of Columbia, Bolivia, Kenya and Ethiopia (not shown). Since these are the only tropical regions with mountains exceeding 4000 m height, it may be speculated that stratiform precipitation there is initiated by large-scale vertical motions along the mountain slope.

Over the extratropics (30°-60°; this latitude range has been chosen since there are virtually neither gauge nor satellite measurements in the GPCP datasets poleward of 60°), there is a distinct annual cycle of precipitation with summer maxima over land and winter maxima over the oceans (not shown). Judged from hemispheric means, the annual amplitude of precipitation is overestimated in all reanalyses, with excessive summer precipitation over land and too little over the oceans of both hemispheres, particularly for NCEP. Probably the differences in the annual cycle are due to enhanced precipitation connected to warm fronts in the models, whereas in reality more precipitation falls along cold fronts. However, this issue has to be left to a detailed examination, since from monthly means no judgement is possible.

The interannual variability of precipitation from different data sources for tropical land and ocean points is discussed next. A 1-2-1 smoother has been applied to the data. An interesting feature is the long-term trend in the ERA data with a slight decrease of precipitation over the tropical land masses and a slight increase over the tropical oceans (Fig. 7). In the late eighties, a similar trend is visible in the GPCP land precipitation. The GPCP satellite estimates over the oceans do not show an increase of precipitation. However, there are some atoll observations in the deep tropics where such an increase is visible (compare Fig. 11 below), whereas in the observational record of other stations no such trend can be found. Over the tropical oceans, the most striking feature in ERA is the large variability of the first guess (between 2.5 mm/day in 1984 and 5.3 mm/day in 1991) and, to a lesser extent, of the 12-24 hour forecasts, in connection with spinup values up to 40% early in 1984. Large variability of precipitation, especially over the oceans where only satellite soundings are available, occurs when there are two satellites in operation, which points towards sampling problems. Also some interannual variations are visible in the ERA data with more precipitation prior to El Niño events and less thereafter. The main contributions come from the tropical oceans. Both long-term trend and interannual variability are very interesting features that should be investigated further. For the moment they are regarded as unrealistic because the other datasets do not show these features.

The interannual variability of precipitation during boreal summer in ERA06 is shown in Fig. 8 in a north-south section of precipitation averaged over a relatively narrow band in east-west direction (15°E-25°E, i.e. Africa and Europe). Around 1987, the position of the ITCZ moves from about 8°N to 2°S. A comparable shift is visible in ERA24 (not shown). A similar plot for the DJF season also shows a shift to the south, but less dramatic. When comparing the different data sources for the two periods 1986/1987 and 1988-1991 (Fig. 9) for the same belt we found for both periods that the ERA values of the ITCZ are much higher than those from GPCP. As mentioned, the position of the ITCZ shifts by 10° to the south between the two periods, the latter one being less reasonable. Soil moisture

chosen from the dataset of Morrissey et al. (1993). In the deep tropics, ERA06 generally comes closest to the observations, although there are large differences for single months. Both ERA06 and ERA24 are superior to the NCEP reanalysis that underestimates strong precipitation events. Differences are generally smaller in the outer tropics where ERA and NCEP are quite similar.

5. Day-by-day variability

Precipitation is highly variable both in time and space and it is therefore very difficult to obtain representative area averages on a daily basis. In Belgium, a very dense observational net exists, which we used for a comparison only with the ERA data. The T106 grid point "Central Belgium" (4.5°E, 51.0°N), covered by 31 observational stations, is compared to the ERA precipitation to represent the day-by-day variability. Fig. 12 shows the daily precipitation for July and December of a 7 year period. Although, for the ease of data handling, all three datasets represent slightly different averaging periods[4)], the correlations between reanalyses and observations are quite high:

December 1981-1987:	Obs. / ERA06	73 %	Obs. / ERA24	68 %,
July 1981-1987:	Obs. / ERA06	70 %	Obs. / ERA24	66 %.

For a grid point near Basel (Switzerland) with even higher observational data density, we find:

January 1983-1991:	Obs. / ERA06	79 %	Obs. / ERA24	78 %,
July 1983-1991:	Obs. / ERA06	66 %	Obs. / ERA24	64 %.

This result is quite encouraging. By choosing larger areas and strictly comparable averaging periods, the scores can probably be improved. The mostly convective summer precipitation is less easy to simulate. The 12-24 hour forecast range scores worse than the 6 hour forecast range for this time scale while for monthly means the longer range forecasts seem to be superior. This agrees with our expectations.

---

4) Observations: 06 UTC to 06 UTC next day, ERA06: 00 UTC to 24 UTC and ERA24: 12 UTC to 12 UTC next day.

data coverage. Also the usage of satellite data in the three-dimensional variational analysis method is quite different from the use of the TOVS as done in the operational analyses in the eighties.

Fig. 15 elucidates the different behaviour of spinup for two areas, northern Europe and northern Australia. Two diurnal cycles are displayed because a 24h forecast starting at 12GMT reaches into the next day. Precipitation values from the forecasts for the first guess (6 hours) is an average which is plotted at 03, 09 UTC and so on. The 24 hour forecast starting at 00 UTC gives four values, at 03, 09, 15, and 21 UTC, and that starting at 12 UTC gives values for 15, 21 UTC and 03, 09 UTC the next day (marked as 27 and 33 GMT). Arpe and Stendel (1996) note that a distinct pattern can be found in the diurnal cycle of the spinup. Regions in which stratiform precipitation spinup dominates (e.g. over Europe in winter) have only a small diurnal cycle of this quantity, and in both 24 hour forecasts (from 00 and 12 UTC) a strong increase is found during the course of the forecasts. On the other hand, there is almost no spinup over northern Australia in the forecast started at 00 UTC, whereas large spinup values are found in the forecast started twelve hours later. The opposite is true for equatorial Africa and large parts of South America. On average, the 12-24 hour forecasts provide an increase compared to the 6 hour forecasts which mean also for this area a better agreement with the GPCP data.

In Fig. 16 the diurnal amplitude of the spinup (forecast started at 00 UTC compared to 12 UTC) is shown. Over tropical land where convective precipitation dominates, the spinup is larger when the initial analysis from which the forecast is started is valid for the evening or the night (Arpe and Stendel, 1996). For boreal summer a similar effect can be seen over Eastern USA and Central Europe. It can be speculated that the diurnal cycle of convective spinup is driven by the soil temperature that cools down too slowly at night, thus favouring convection. An important exception can be noticed during summer monsoon over western India where the forecast starting at 00 UTC (=04 local time) has a much larger spinup than that from 12 UTC. This may be due to the fact that enough soil moisture is available during the summer monsoon season so that convection here is mainly driven by the diurnal cycle of insolation. Over the tropical Pacific, the spinup of the forecast starting at 12 UTC (near local midnight) is considerably larger than that from 00 UTC, consistent with the well-known nocturnal or early morning rainfall maximum (Chang et al., 1995, see also Kraus, 1963).

Table 2 compares precipitation and evaporation sums from different sources for land and oceans. Due to the lack of observational data, considerable discrepancies exist in the different datasets, and the quality of the evaporation fields in the reanalyses is difficult to judge, especially over the oceans, where evaporation rates are at best known within 30% (Oberhuber, 1988). However, from the considerations above, there is some evidence that gradients are too weak in the NASA reanalysis, i.e. there is too much evaporation in arid regions and not enough in the tropics.

	P_{Land}	E_{Land}	$P\text{-}E_{Land}$	P_{Ocean}	E_{Ocean}	$P\text{-}E_{Ocean}$	P_{global}	$P\text{-}E_{global}$
ERA06	114	83	31	383	429	-46	497	-15
ERA24	123	83	40	426	441	-15	549	25
Spinup	9	0	9	43	12	31	52	40
NCEP	121	95	26	384	410	-26	505	0
NASA	118	118	0	370	364	6	488	6
ECHAM4	113	77	36	408	445	-37	521	-1
GPCP G/S	109	-	-	395	-	-	504	-
Schemm	107	-	-	396	-	-	503	-
Baumg.	111	71	40	385	424	-39	496	1
Chahine	107	71	36	398	434	-36	505	0
Hartmann	111	71	40	388	428	-40	499	0
Legates	121	-	-	464	-	-	585	-
Jaeger	109	-	-	380	-	-	489	-

Table 2: Components of the hydrological cycle [10^{15} kg a^{-1}]*) for the period 1988-1993. P stands for precipitation and E for evaporation. GPCP G/S is the mixed raingauge/satellite estimate from GPCP, Schemm stands for a blend of conventional observations over land (Schemm et al., 1992) and MSU estimates over the oceans (Spencer, 1993). Other estimates from Baumgartner and Reichel (1975), Chahine (1992) and Hartmann (1994). Also shown are the climatologies from Legates and Willmott (1990) and Jaeger (1976) and a simulation with ECHAM4 (T42, observed monthly mean SST).

*) Over land (ocean), 1mm/day is equivalent to 54.605 (131.746) $\cdot 10^{15}$ kg a^{-1}. For the globe, 1 mm/day equals $186.314 \cdot 10^{15}$ kg a^{-1}.

While there is general agreement about the land precipitation, the uncertainty of oceanic precipitation is much larger. It can be seen that, on a global scale, there is a lack of precipitation during the early stages of the forecast (ERA06), while in ERA24 a considerable amount of water is accumulated. It turned out during the creation of the ECMWF reanaly-

Paraná region), South Africa and Australia also exhibit this imbalance. The deficit is particularly large in the Peru/Ecuador area and over parts of South Africa, with values up to 4 mm/day.

8. River runoff in the ERA data

For several rivers the observed monthly mean runoff is available (Dümenil et al., 1993), and we have used these data to check the long term mean of P-E from the reanalyses. The Amazonas and the Mackenzie, two slowly flowing rivers, are selected here for demonstration. In light of the uncertainty of the observations, the ERA precipitation data are reasonable for both river catchment areas (Fig. 20), while NCEP data provide an overestimate especially in summer for the Mackenzie river. The evaporation in NCEP is much higher than in the ERA data, and from the following we believe that the latter are more correct.

We have compared the P-E of the reanalyses to the observed river discharge. The maximum discharge at the mouth of the Amazonas is found a few months after the maximum precipitation further upstream. For the Mackenzie, the snow melt in May/June dominates the discharge peak. Such delays of discharge are not yet modelled, and therefore only annual means of P-E and river discharge can be compared. For both rivers the ERA24 data provide nearly exact estimates of the observations, while NCEP is on the low side. For the Mackenzie river basin the ERA06 values are clearly too low, which confirms our finding from above that in the extratropics a longer forecast range gives more realistic precipitation values.

9. Discussion

Considerable efforts have been undertaken recently to improve our knowledge of the hydrological cycle. Available ground-based and satellite observations are being merged in the GPCP project. Several institutions are re-analyzing atmospheric datasets by means of forecast models that do not suffer from the numerous changes in the data assimilation or the model itself that are common to operational analyses.

algorithms were modified several times in the past to keep pace with the advent of more sophisticated instruments and methods. The SSM/I soundings may serve as a relatively accurate database for precipitable water over the oceans (e.g., Liu et al., 1992) that can therefore be used for the validation of the hydrological cycle in the reanalyses. These are, however, available only relatively recently. For the few atoll observations which are assumed to be representative for the ocean, the ERA06 data gives slightly better results than ERA24. More precipitation than estimated from satellites is indicated over oceanic regions where cold upwelling is found (Benguela Current, Humboldt Current). However, these fail to detect low precipitation rates, as by drizzle. Reasonable agreement is found with ship observations (da Silva et al., 1994).

Humidity analysis has always been a matter of concern for numerical weather prediction. In the course of the years, numerous changes have been applied to the treatment of humidity in the operational analyses of the ECMWF, resulting in large temporal inconsistencies of humidity variables (Arpe, 1990). These are discussed to some extent e.g. in Trenberth (1992). Although a frozen model version is used in the reanalysis, humidity variations cannot be expected to be entirely natural, since errors in other quantities may also affect humidity, as discussed in section 7. Observational methods have changed as well, and there was a steady increase of the number of available observations from aircrafts and satellites, so that the large fluctuations of precipitation are probably caused by a combination of all these factors.

10. Conclusions

For monitoring the climate change, temporal consistent datasets are extremely important. The spatial and temporal distribution of precipitation is of most vital interest. Considerable efforts have been made in order to obtain such precipitation data, both by incorporation of gauge measurements and satellite soundings and by means of creating consistent model-based forecast data to close the gaps that cannot be filled by conventional or satellite observations.

Although there are some characteristic differences between the three reanalyses that were examined in detail, their consistency has much improved as compared e.g. to ECMWF's operational analyses. This can be seen in the time series that were presented in section 4 as well as in the latitude-time series of the vertical velocity. However, none of the reanalyses is perfect.

Acknowledgements

This study has been carried out within the ECMWF reanalysis validation project which is supported by the EC project No. EV5V-CT93-0286. We thank R. Gibson, P. Kållberg, S. Uppala and A. Nomura from the ECMWF reanalysis group for making available the ECMWF reanalysis data to us. A. Chang provided us with SSM/I emission precipitation data and G.J. Huffman with the merged GPCP data. We are also indebted to B. Rudolf for making available the preliminary GPCC dataset. Microwave precipitation estimates were supplied by R.W. Spencer. We would also like to thank L. Bengtsson, P. Kållberg and M. Christoph for useful discussions about the quality of the different datasets and comments that helped to clarify the script.

References

Adler, R.F., H.-Y. M. Yeh, N. Prasad, W.-K. Tao, J. Simpson, 1991: Microwave simulations of a tropical rainfall system with a three-dimensional cloud model, *J. Appl. Met.*, **30**, 924-953.

Adler, R.F., G.J. Huffman and P.R. Keehn, 1994: Global rain estimates between large-scale convective rainfall and cold cloud over the Western Hemisphere during 1982-1984, *Mon. Wea. Rev.*, **115**, 51-74.

Arakawa, A. and W. Schubert, 1974: Interaction of a cumulus ensemble with the large-scale environment, part I, *J. Atm. Sci.*, **31**, 674-701.

Arkin, P.A. and B.M. Meisner, 1987: The relationship between large-scale convective rainfall and cold cloud over the western hemisphere during 1982-1984, *Mon. Wea. Rev.*, **115**, 51-74.

Arpe, K., 1990: Impacts of changes in the ECMWF anaysis-forecasting scheme on the systematic error of the model, *Proceedings of the ECMWF Seminar "Ten years of medium range weather forecasting"*, 4-8 September 1989, Reading, UK, 69-114.

Arpe, K., 1991: The hydrological cycle in the ECMWF short range forecasts, *Dyn. Atmos. Oceans*, **16**, 33-59.

Arpe, K., L. Bengtsson, L. Dümenil and E. Roeckner, 1994: The hydrological cycle in the ECHAM3 simulations of the atmospheric circulation, in: M. Desbois and F. Désalmand (Eds.): *Global precipitations and climate change*, NATO ASI Series, Vol **I 26**, p. 361-377.

Arpe, K. and H. Cattle, 1993: A comparison of surface stress and precipitation fields in short-range forecasts over the Antarctic region, *J. Geophys. Res.*, **98**, 13035-13044.

Huffman, G.J., R.F. Adler, P.A.Arkin, A. Chang, R. Ferraro, A. Gruber, J. Janowiak, R.J. Joyce, A. McNab, B. Rudolf, U. Schneider and P. Xie, 1996: The Global Precipitation Climatology Project (GPCP) combined precipitation data set, subm. to *Bull. Am. Met. Soc.*

Jaeger, L., 1976: Monatskarten des Niederschlags für die ganze Erde, *Berichte des Deutschen Wetterdienstes*, Nr. **139(18)**, Offenbach a.M., 38 pp.

Janowiak, J.E. and P.A. Arkin, 1991: Rainfall variations in the tropics during 1986-1989, as estimated from observations of cloud-top temperatures, *J. Geophys. Res.*, **96**, 3359-3373.

Kalnay, E., M. Kanamitsu, R. Kistler, W. Collins, D. Deaven, L. Gandin, S. Saha, G. White, J. Woollen, M. Chelliah, J. Janowiak, K.C. Mo, J. Wang, A. Leetma, R. Reynolds, R. Jenne, E. Kung and D. Salstein, 1993: The NMC/NCAR CDAS reanalysis project, *NMC Office Note* **401**, available from NMC/NWS/NOAA, Washington D.C., 20233, 288 pp.

Kalnay, E., M. Kanamitsu, R. Kistler, W. Collins, D. Deaven, J. Derber, L. Gandin, S. Saha, G. White, J. Woollen, Y. Zhu, M. Chelliah, W. Ebisuzaki, W. Higgins, J. Janowiak, K.C. Mo, C. Ropelewski, J. Wang, A. Leetma, R. Reynolds and R. Jenne, 1995: The NMC/NCAR 40-year reanalysis project, *Bull. Amer. Met. Soc.*, **77**, 437-473.

Kraus, E.B., 1963: The diurnal precipitation change over the sea, *J. Atm. Sci.*, **20**, 551-556.

Krishnamurti, T.N., J. Xue, H.S. Bedi, K. Ingles, D. Oosterhof, 1991: Physical initialization for numerical weather prediction over the tropics, *Tellus*, **43AB**, 53-81.

Legates, D.R., 1987: A climatology of global precipitation, *Publ. in Climatology*, **40**(1), Newark, Delaware, 85 pp.

Legates, D.R. and C.J. Willmott, 1990: Mean seasonal and spatial variability in gauge corrected global precipitation, *J. Clim.*, **10**, 111-127.

Liu, W.T., W. Tang and F. Wentz, 1992: Precipitable water and surface humidity over global oceans from Special Sensor Microwave Imager and European Centre for Medium-Range Weather Forecasts, *J. Geophys. Res.*, **97**, 2251-2264.

Lott, F. and M. Miller, 1995: A new sub-grid scale orographic deag parameterization: its formulation and testing, subm. to *Quart. J. R. Met. Soc.*

Mintz, Y. and Y.V. Serafini, 1989: Global monthly climatology of soil moisture and water balance, *Note Interne LMD* No. **148**, Ecole Polytechnique, Palaiseau.

Mo, K.C. and R.W. Higgins, 1995: Large scale atmospheric water vapor transport as evaluated from the NMC/NCAR and the NASA/DAO reanalyses, subm. to *J. Climate*.

Molod, A., H.M. Helfand and L.L. Takacs, 1995: The climatology of parameterized physical processes in the GEOS-1 GCM and their impact on the GEOS-1 data assimilation system, subm. to *J. Climate*

Moorthi, S. and M.J. Suarez, 1992: Relaxed Arakawa-Schubert: A parameterization of moist convection for general circulation models, *Mon. Wea. Rev.*, **120**, 978-1002.

Schemm, J., S. Schubert, J. Terry and S. Bloom, 1992: Estimates of monthly mean soil moisture for 1979-1989. *NASA Tech. Memo.*, **104571**, 262pp.

Schneider, U., H. Hauschild, M. Reiss and B. Rudolf, 1992: Erste Vergleiche der aus täglichen Vorhersagen des EZMF-Modells T106 und aus konventionellen Meßdaten abgeleiteten monatlichen Gebietsniederschläge, *Meteor. Z.*, N.F. **1**, 66-72.

Schubert, S.D. and Y. Chang, 1996: An objective method for inferring sources of model error, *Mon. Wea. Rev.*, **124**, 325-340.

Schubert, S.D., J. Pfaendtner and R. Rood, 1993: An assimilated data set for earth science applications, *Bull. Amer. Met. Soc.*, **74**, 2331-2342.

Spencer, R.W., 1993: Global oceanic precipitation from the MSU during 1979-91 and comparisons to other climatologies, *J. Clim.*, **6**, 1301-1326.

Stendel, M., 1993: Diagnostische Studien zur Darstellung frontaler Strukturen in einem mesoskaligen Vorhersagemodell, *Mitteilungen aus dem Institut für Geophysik und Meteorologie der Universität zu Köln*, Heft **96**, 152 pp.

Stendel, M. und K. Arpe, 1996: Evaluation of the hydrological cycle in reanalyses and observations, *Proceedings of the Second International Scientific Conference on the Global Energy and Water Cycle*, 17.-21. Juni 1996, Washington, DC, 46-47.

Takacs, L.L., A. Molod and T. Wang, 1994: Documentation of the Goddard Earth Observing System (GEOS) General Circulation Model (GCM) - Version I., NASA Tech. Memo., **104606**, Vol. 1.

Tiedtke, M., 1993: Representation of clouds in large-scale models, *Mon. Wea. Rev.*, **121**, 3040-3061.

Trenberth, K.E., 1992: Global analyses from ECMWF and atlas of 1000 to 10 mb circulation statistics, *NCAR Tech. Note* NCAR/TN-**373**+STR, 191 pp.+24 fiches.

Trenberth, K.E. and J.G. Olson, 1988: Intercomparison of NMC and ECMWF global analyses: 1980-1986, *NCAR Tech. Note* NCAR/TN-**301**+STR, 81 pp.

Viterbo, P., 1995: Initial values of soil water and the quality of summer forecasts, *ECMWF Newsletter*, **69**, 2-8.

Viterbo, P. and A.C.M. Beljaars, 1995: A new land surface parameterization scheme in the ECMWF model and its validation, *ECMWF Tech. Rep.*, **75**.

Weng, F. and N.C. Grody, 1994: Retrieval of cloud liquid water using the Special Sensor Microwave Imager (SSM/I), *J. Geophys. Res.*, **99**, 25535-25551.

Wilheit, T., A. Chang and L. Chiu, 1991: Retrieval of monthly rainfall indices from microwave radiometric measurements using probability distribution function, *J. Atmos. Ocean. Tech.*, **8**, 118-136.

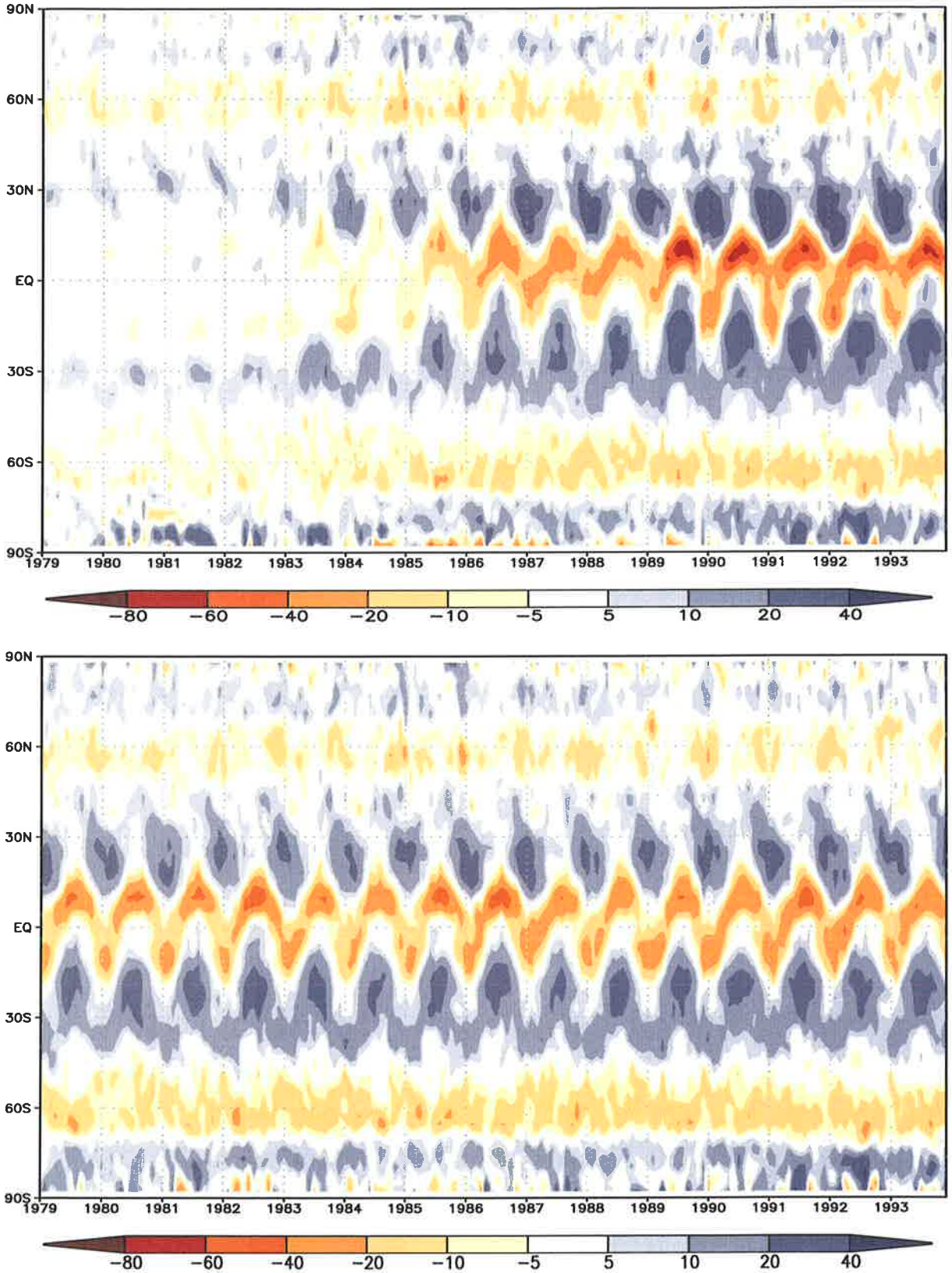

Fig. 1: Latitude-time section (1979-1993) of the zonally averaged vertical velocity ω in 500 hPa. Upper panel: ECMWF operational analyses, lower panel: ECMWF reanalyses. Units: mPa/s.

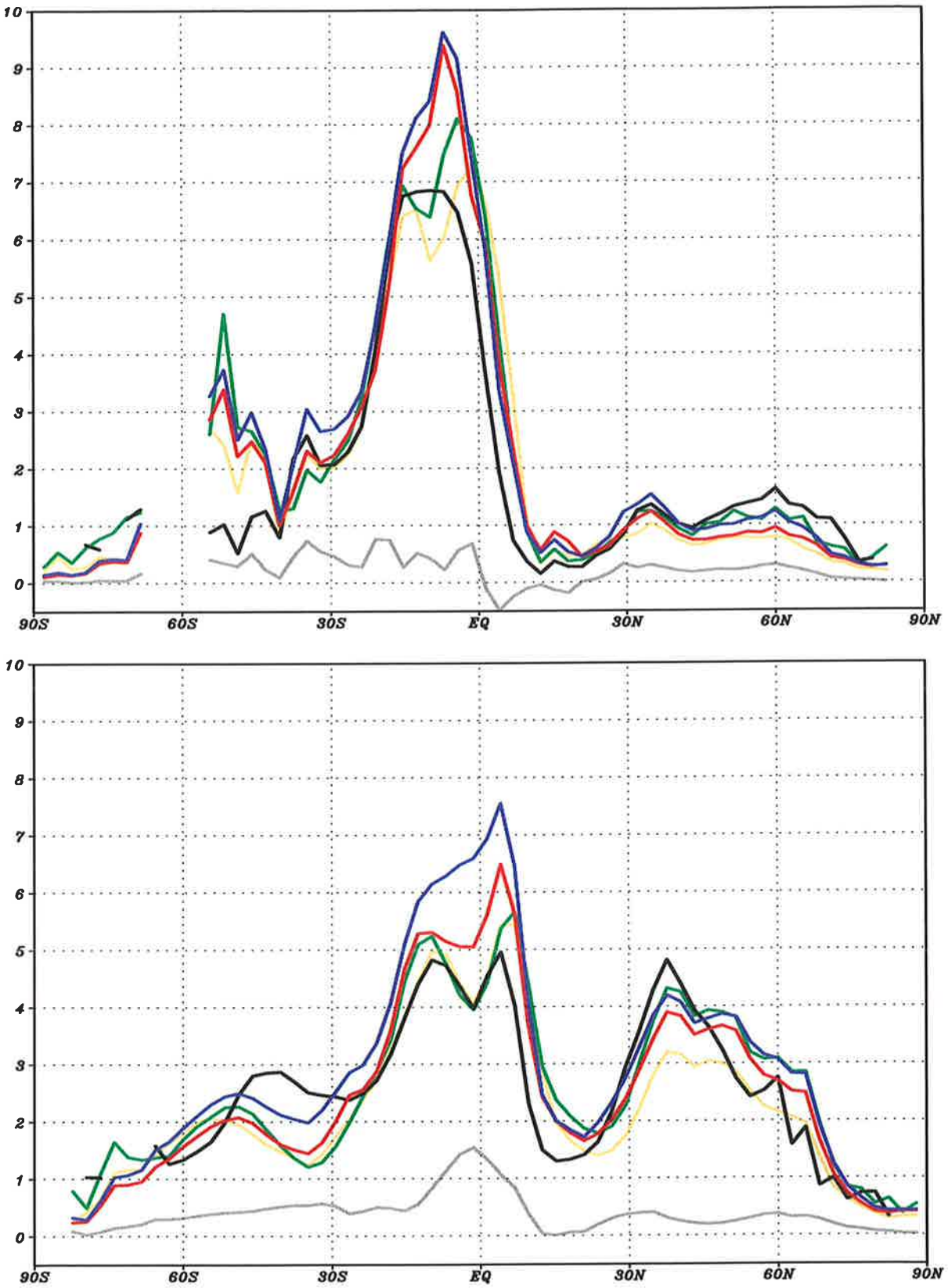

Fig. 2: (a) Meridional cross-section of precipitation in winter (DJF 1988/89 to 1992/93). Top panel: land points, bottom panel: ocean points. Red curve: ERA 06 h forecast, blue curve: ERA 24 h forecast, grey curve: spinup, black curve: GPCP satellite/gauge estimate, green curve: NCEP reanalysis, yellow curve: NASA reanalysis. Units: mm/day.

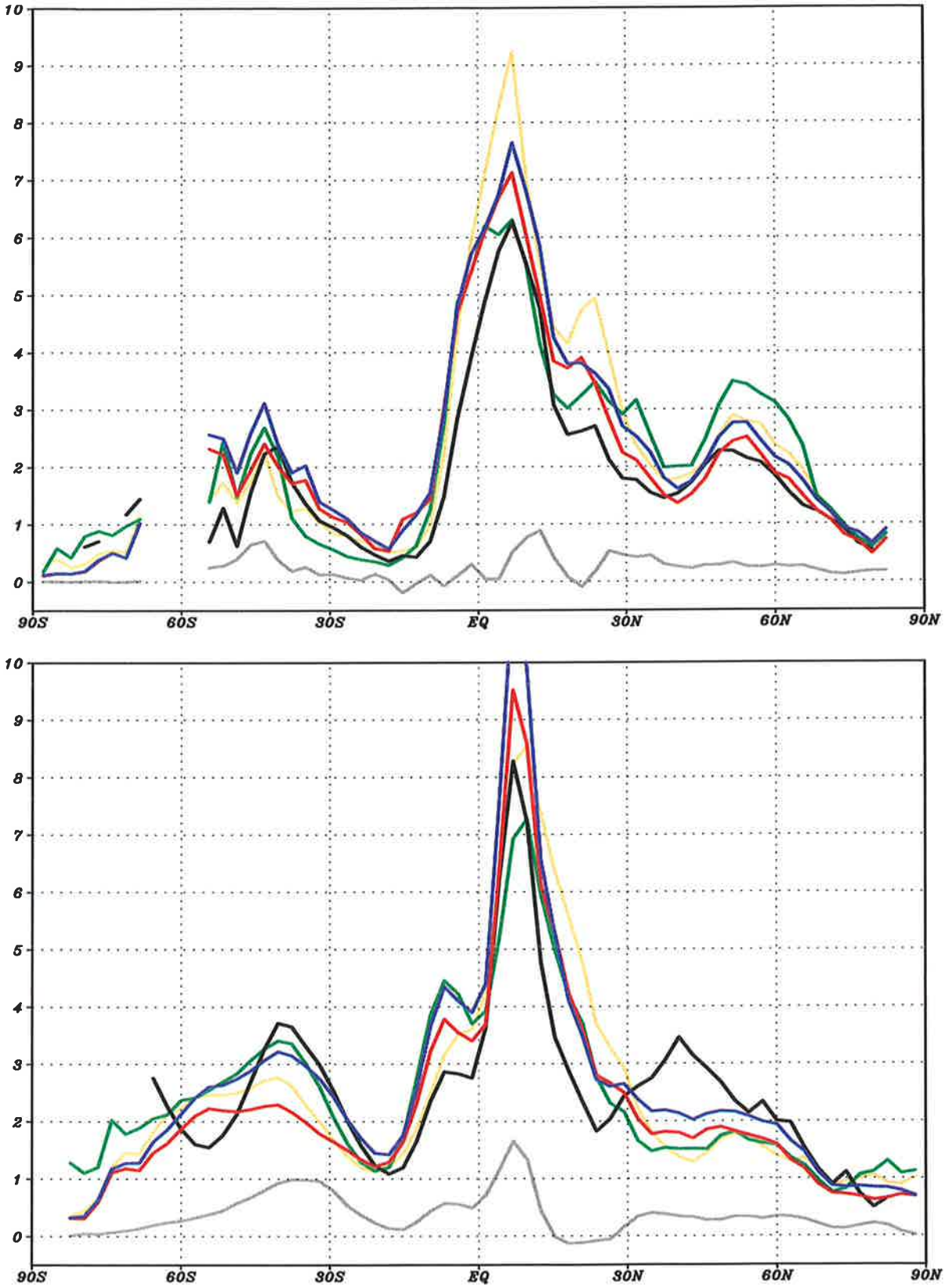

Fig. 2: (b) Meridional cross-section of precipitation in summer (JJA 1988 to 1993). Top panel: land points, bottom panel: ocean points. Red curve: ERA 06 h forecast, blue curve: ERA 24 h forecast, grey curve: spinup, black curve: GPCP satellite/gauge estimate, green curve: NCEP reanalysis, yellow curve: NASA reanalysis. Units: mm/day.

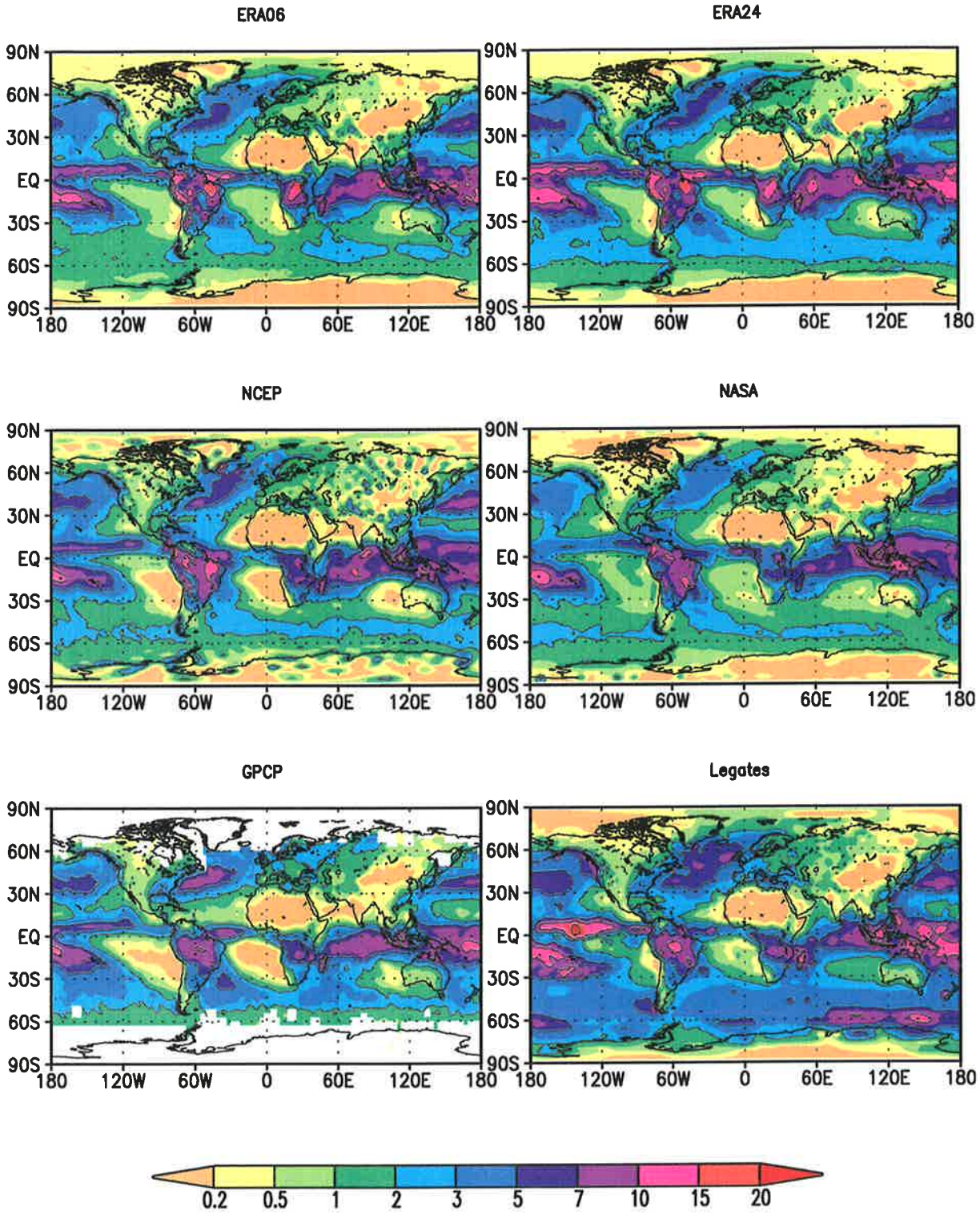

Fig. 3: (a) Total precipitation in winter (DJF 1988/89 to 1992/93). Top left: ECMWF reanalysis (ERA06), top right: ECMWF reanalysis (ERA24), center left: NCEP reanalysis, center right: NASA reanalysis, bottom left: GPCP mixed satellite/gauge estimate, bottom right: Legates and Willmott (1990) climatology. Units: mm/day. Contours at 2, 6 and 10 mm/day.

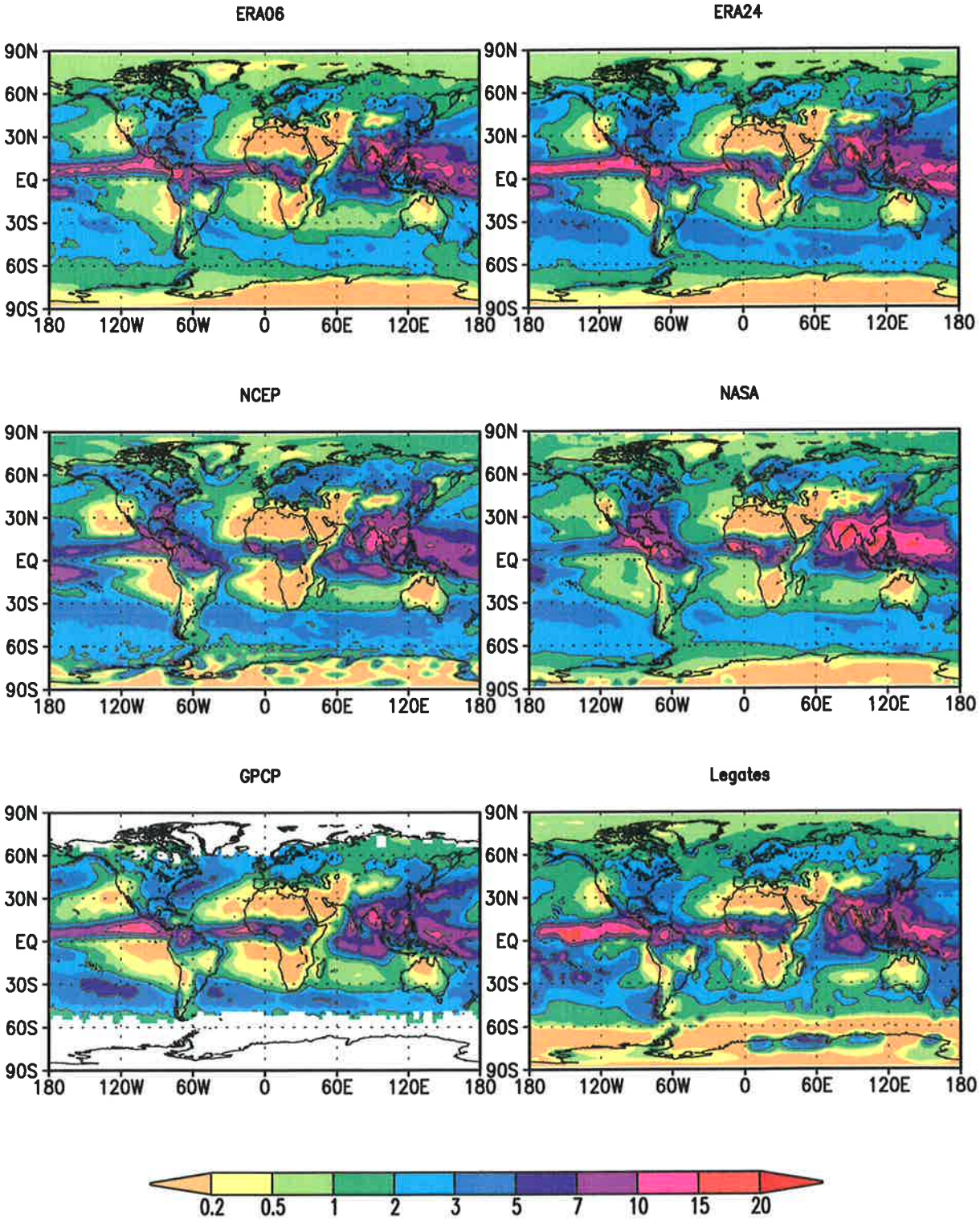

Fig. 3: (b) Total precipitation in summer (JJA 1988 to 1993). Top left: ECMWF reanalysis (ERA06), top right: ECMWF reanalysis (ERA24), center left: NCEP reanalysis, center right: NASA reanalysis, bottom left: GPCP mixed satellite/gauge estimate, bottom right: Legates and Willmott (1990) climatology. Units: mm/day. Contours at 2, 6 and 10 mm/day.

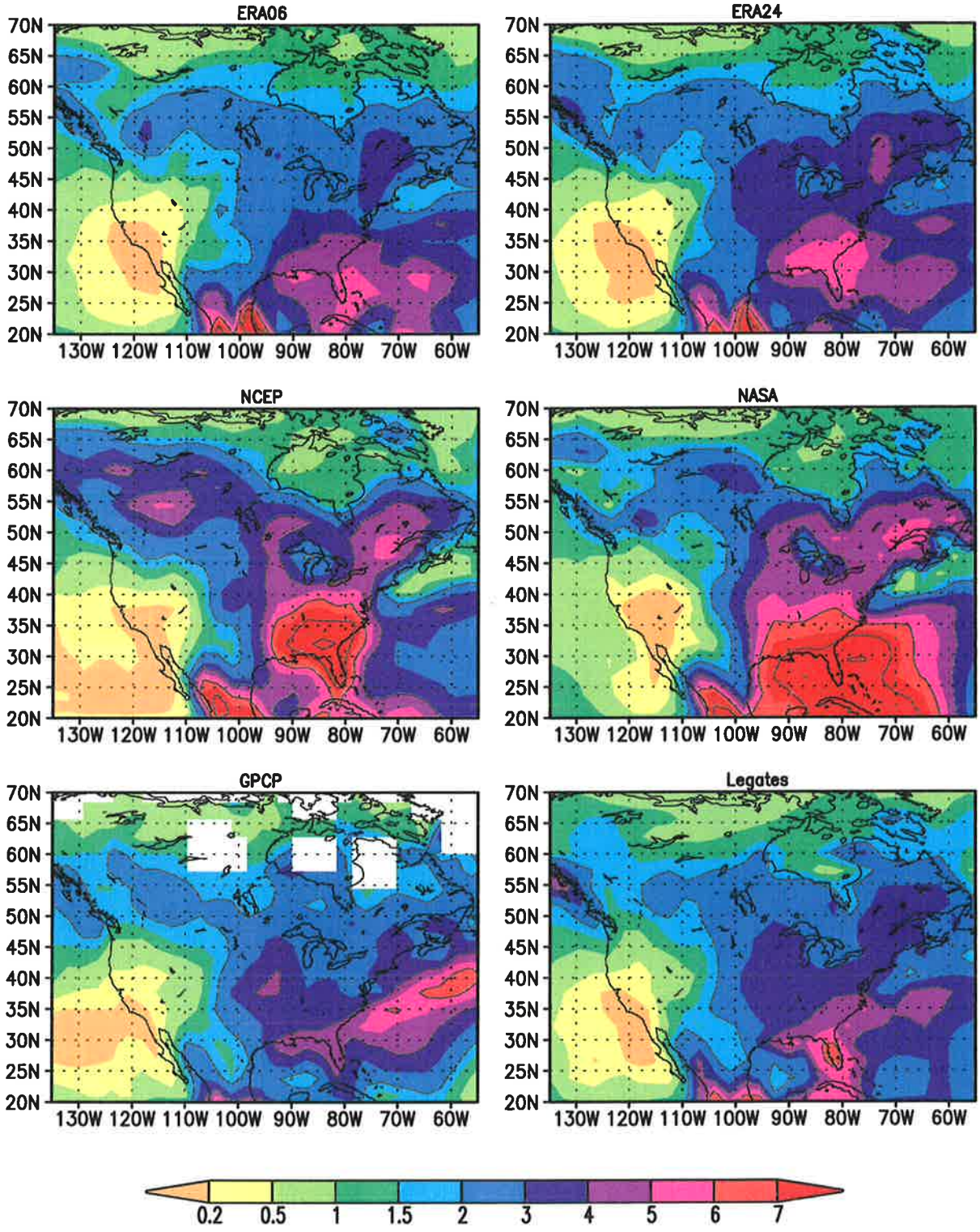

Fig. 4: As Fig. 3, for summer precipitation (JJA 1988-1993) over North America. Contour interval 2 mm/day.

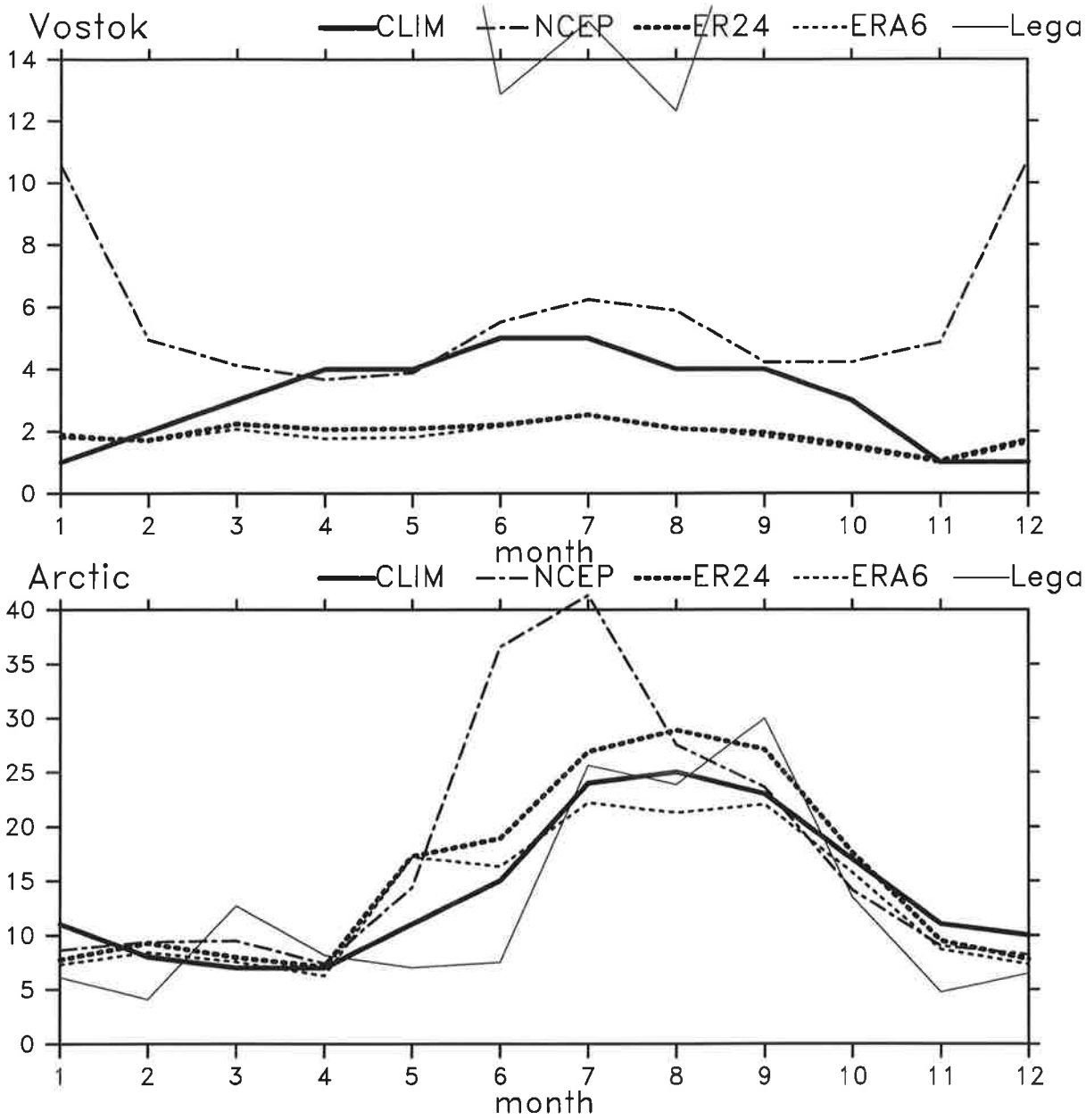

Fig. 5: Annual cycles of precipitation in the polar regions. Upper panel: Vostok (78°27'S, 106°52'E), lower panel: Arctic basin. Climatologies from Genthon and Braun (1995) and Radionov (to be published), respectively. Units: mm/month.

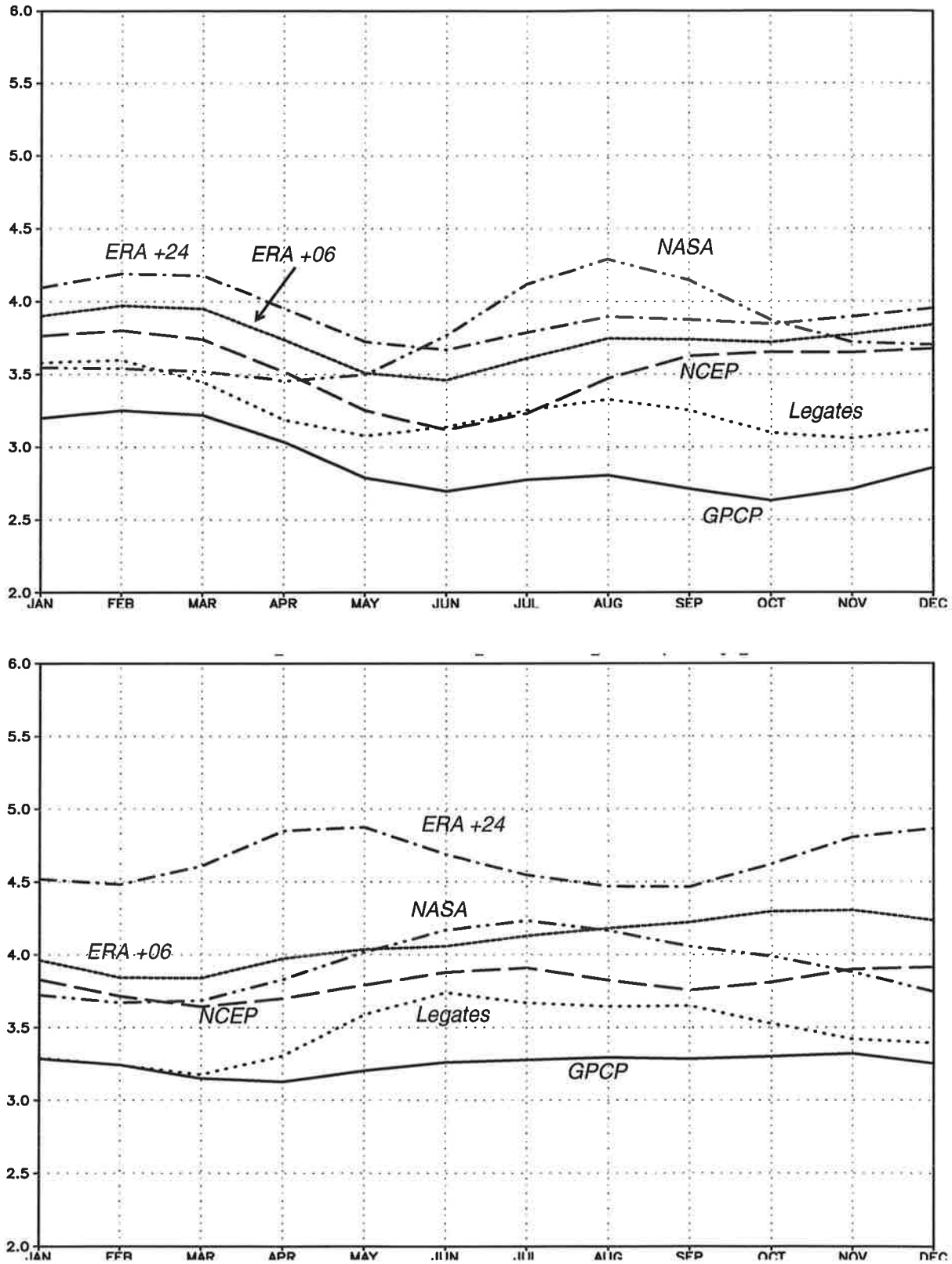

Fig. 6: Annual cycle of precipitation over tropical land masses (upper panel) and tropical oceans (lower panel). Units: mm/day.

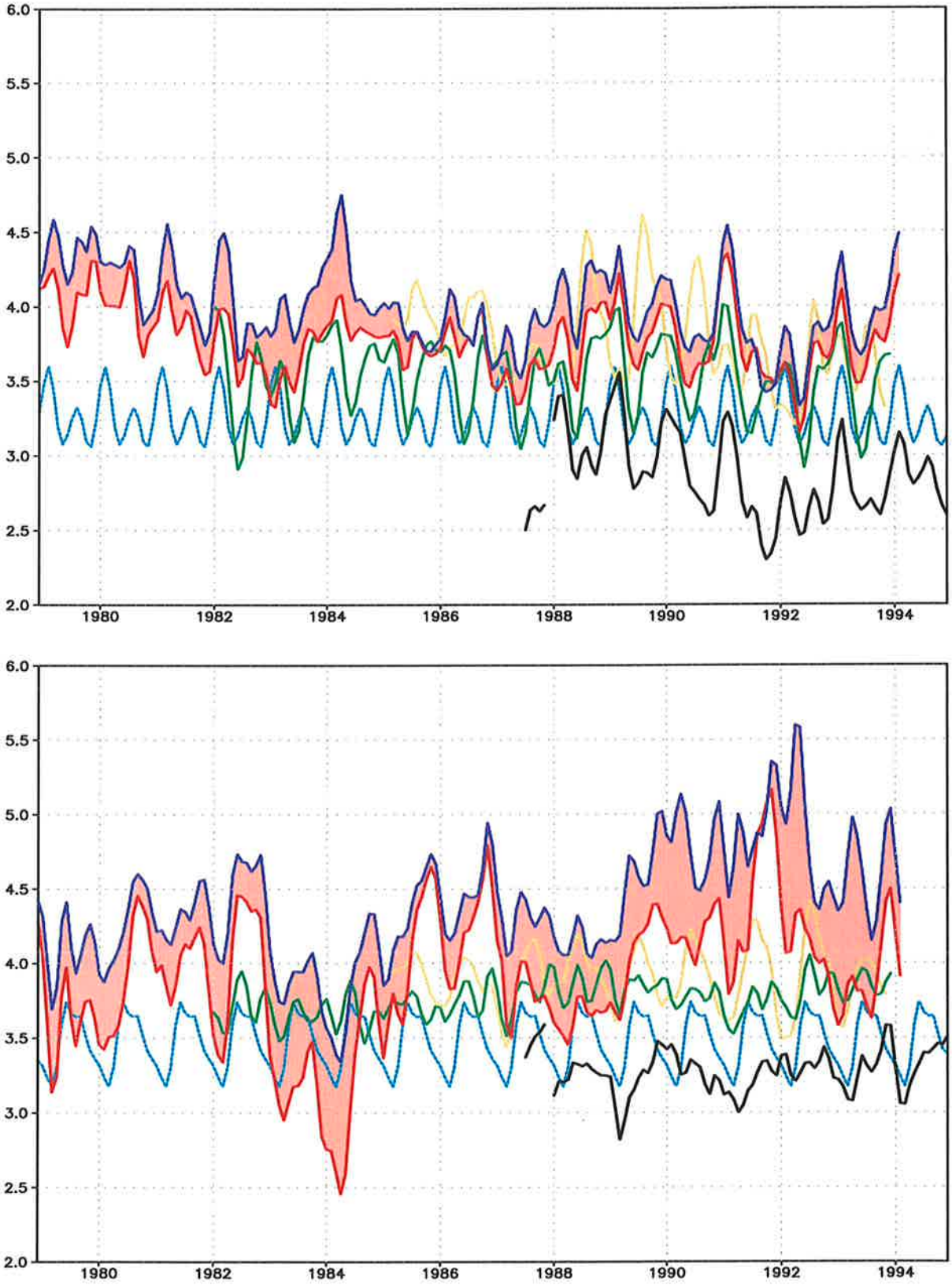

Fig. 7: Time series (1979-1993) of total precipitation over tropical land (upper panel) and over tropical oceans (lower panel). Red line: ERA06, dark blue line: ERA24, shaded area: ERA spinup, green line: NCEP, yellow line: NASA, light blue line: Legates climatology, black line: GPCP satellite/gauge estimate. Units: mm/day.

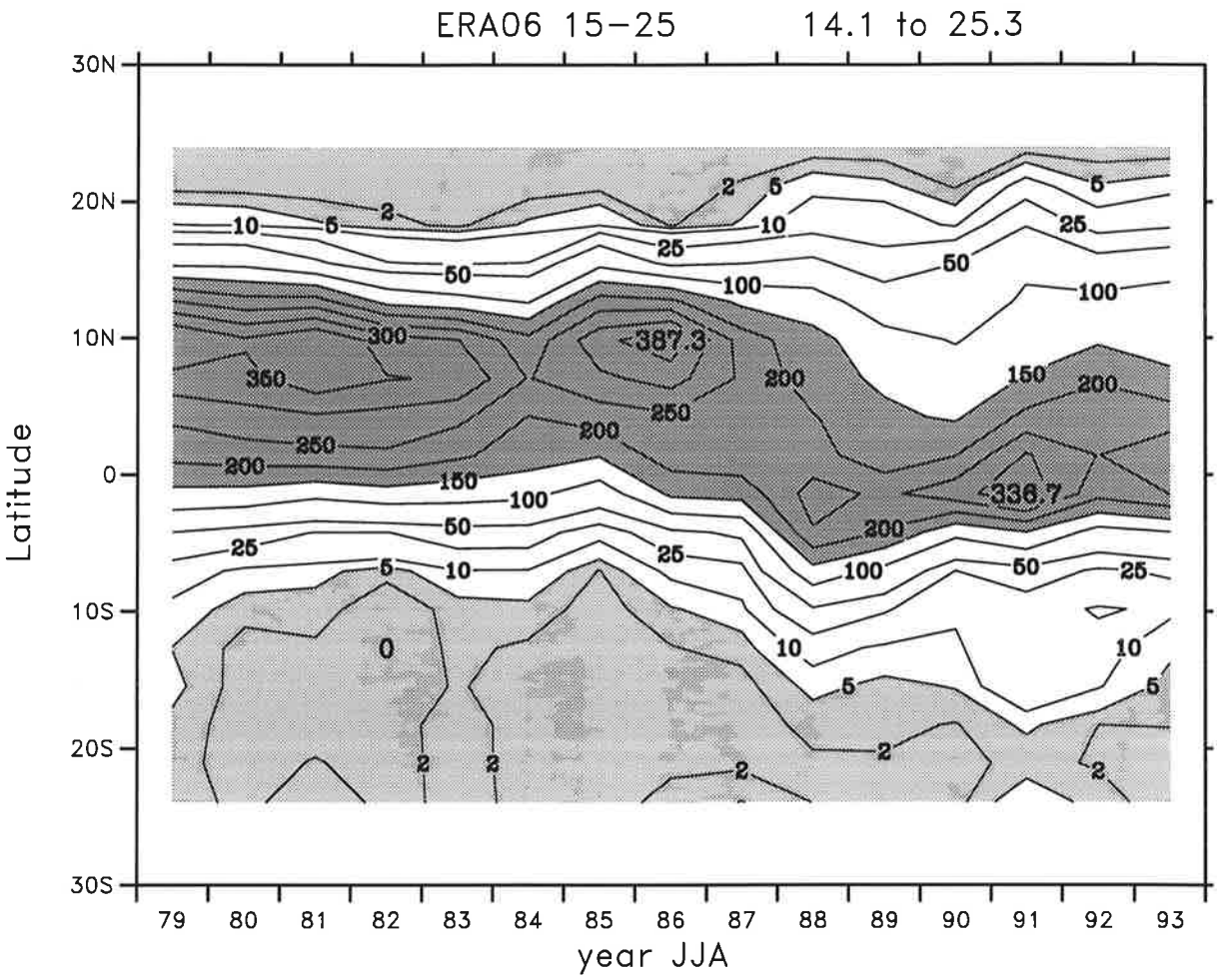

Fig. 8: Latitude-time section of summer (JJA 1979-1993) precipitation in the European/African sector (15°E-25°E). Units: mm/month.

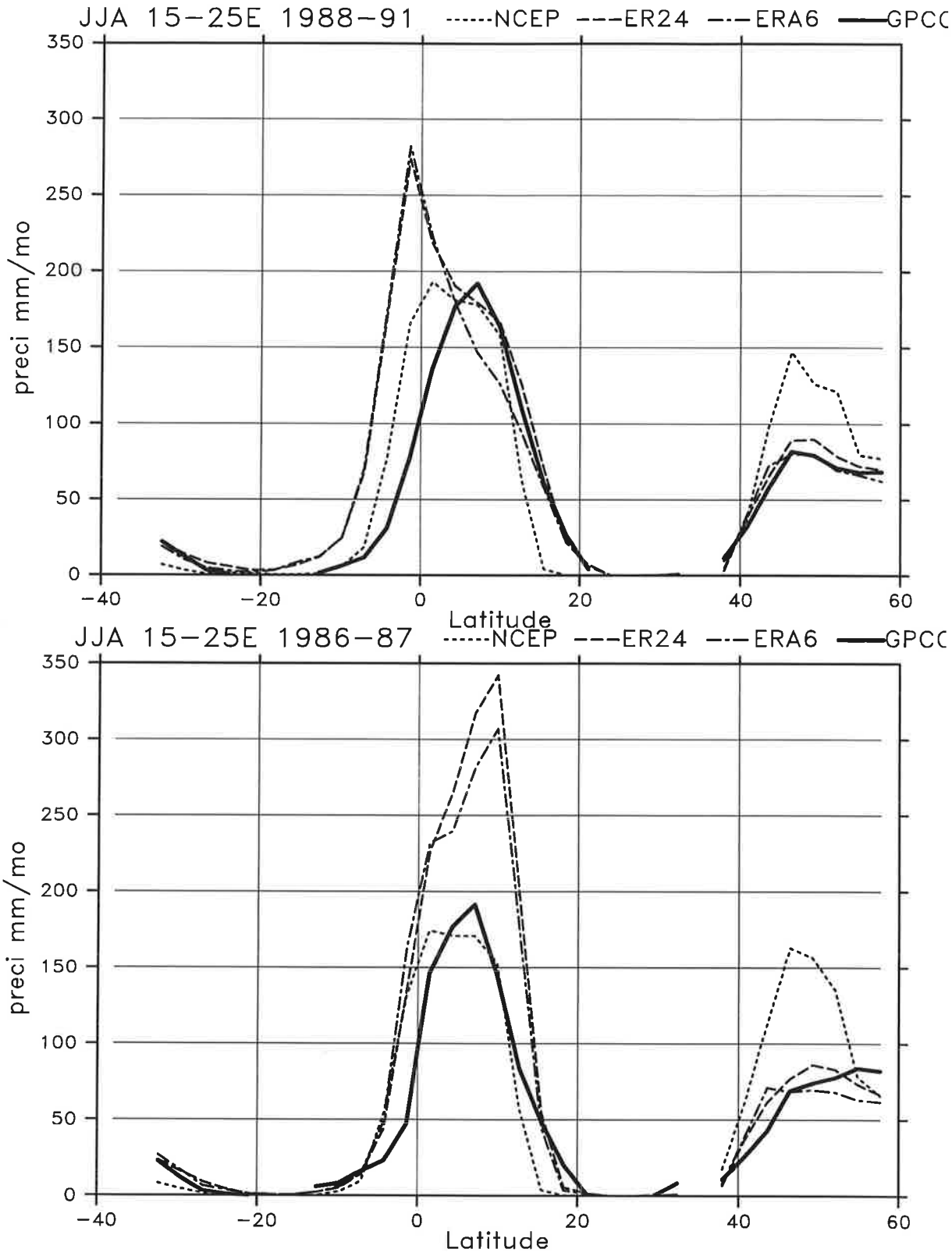

Fig. 9: Meridional cross-section of precipitation averaged from 15°E to 25°E. Upper panel: average for JJA 1988-1993, lower panel: average for JJA 1986/1987. Units: mm/ month.

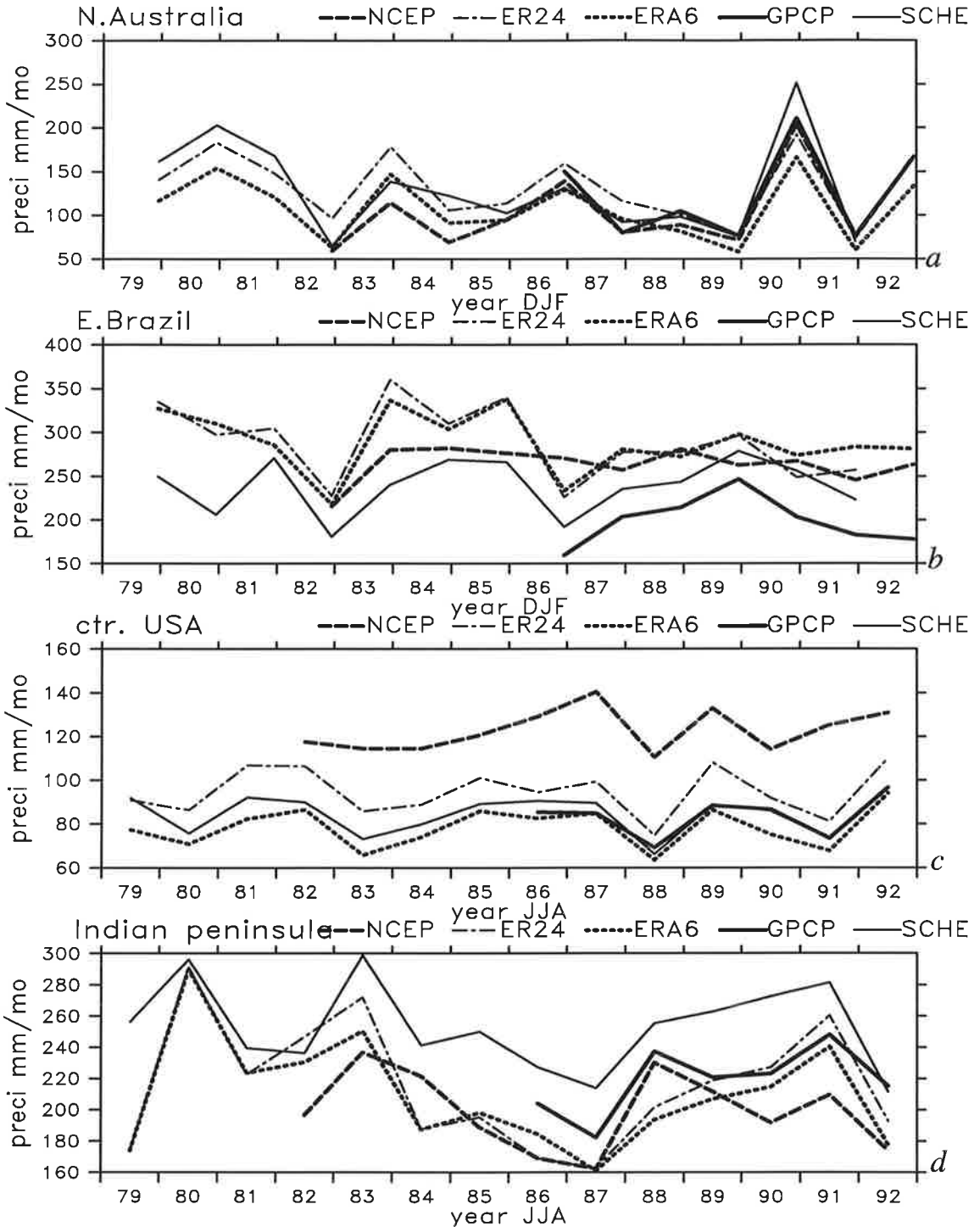

Fig. 10: Time series (1979-1993) of total precipitation for selected regions: (a) Northern Australia (22°S-15°S, 115°E-155°E), (b) Eastern Brazil (10°S-5°N, 60°W-40°W), (c) Central USA (35°N-50°N, 100°W-80°W), (d) Indian peninsula (9°N-21°N, 65°E-90°E, land points only). Units: mm/day.

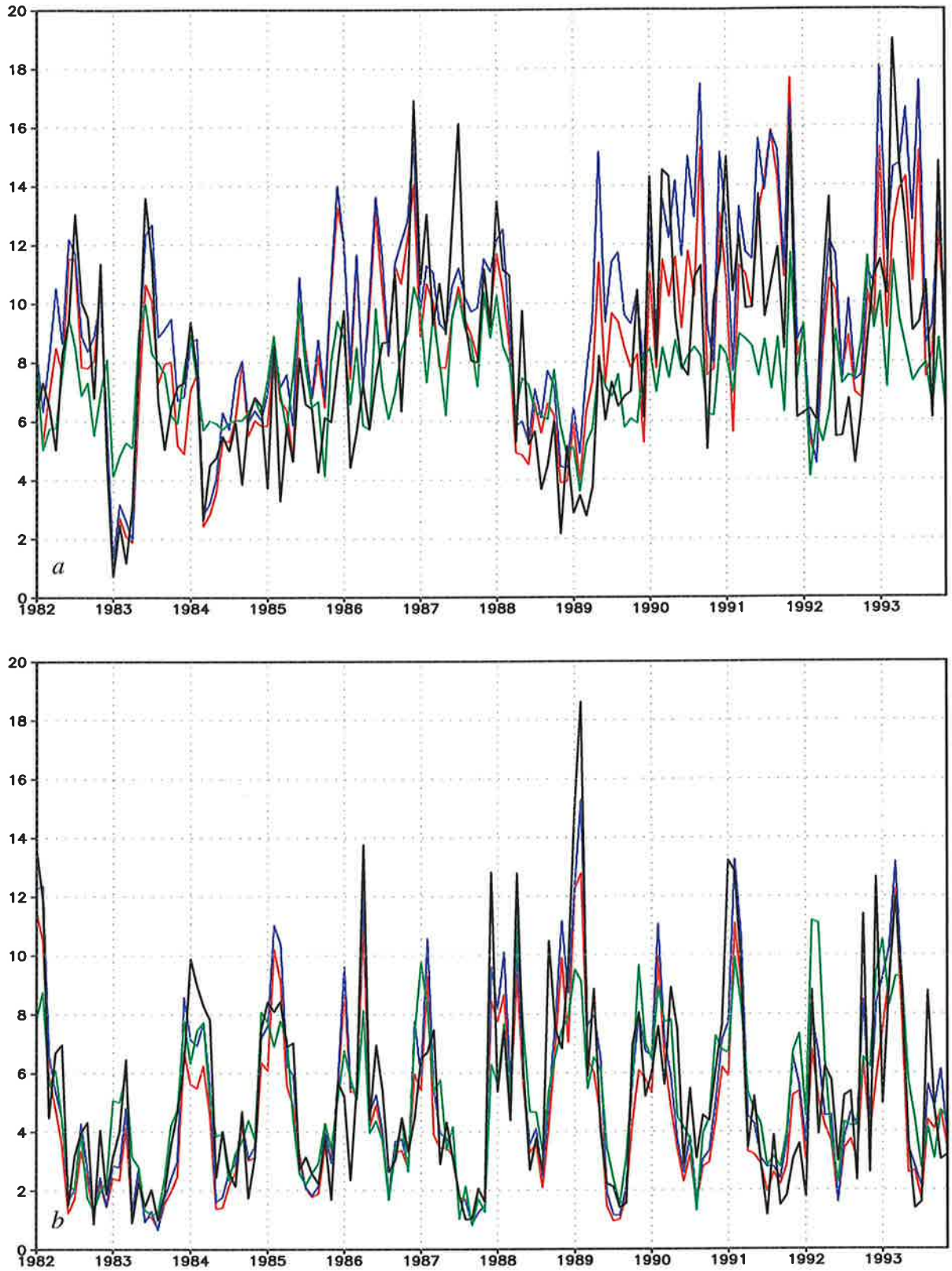

Fig. 11: Time series (1982-1993) of Pacific atoll precipitation (Morrissey et al., 1993, updated, black line) and the corresponding grid points from ERA06 (red) ERA24 (blue) and NCEP (green). (a) average for Majuro (7.1°N, 171.2°E), Tarawa (1.2°N, 172.6°E) and Butaritari (3.0°N, 172.5°E), (b) average for Fua'amotu Apt. (21.1°S,165.1°W), Keppel Is. (15.6°S, 173.5°W) and Alofi (19.0°S, 169.6°W). Units: mm/day.

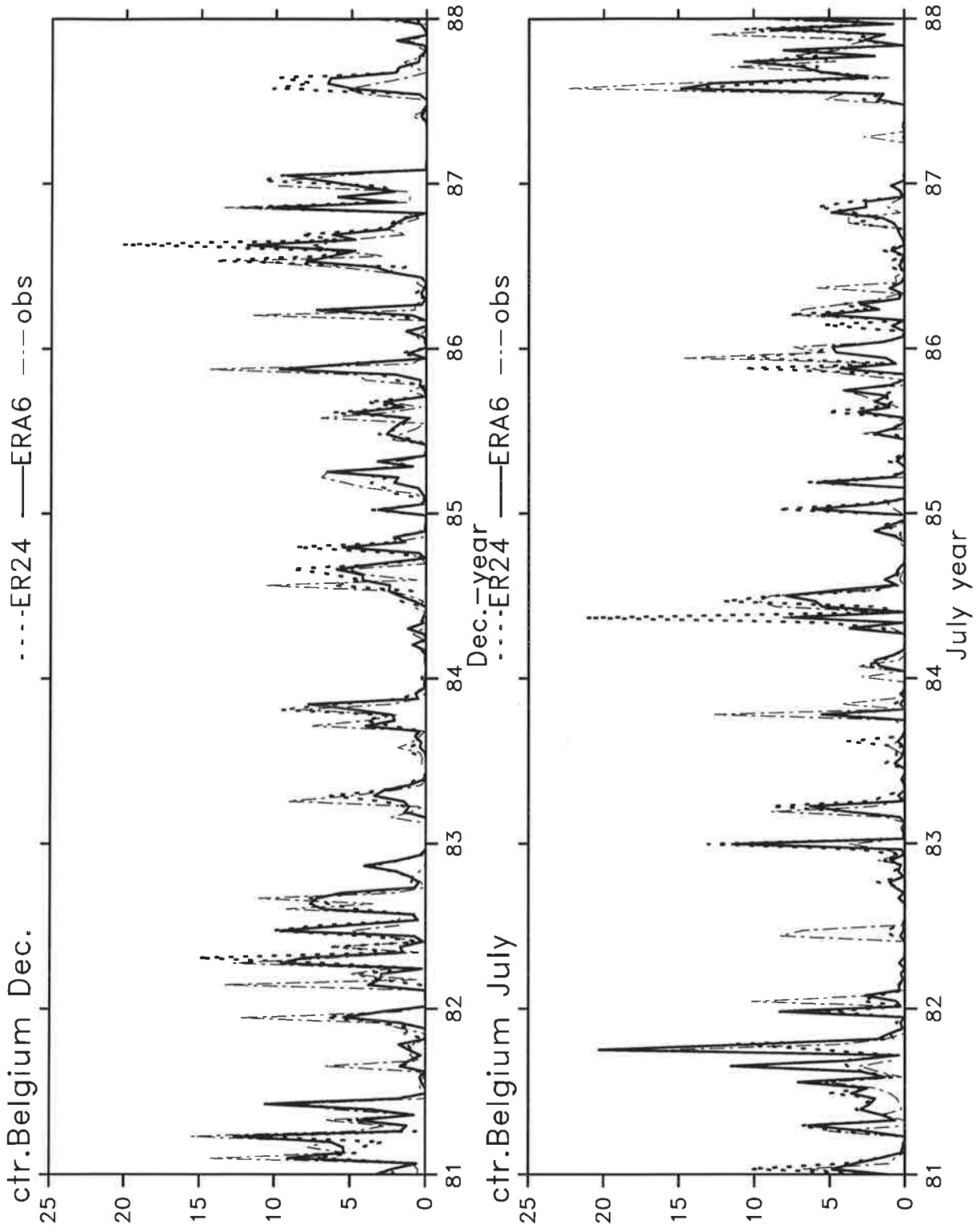

Fig. 12: Time series of daily precipitation in central Belgium for ERA06, ERA24 and observations. Upper panel: December 1981-1987, lower panel: July 1981-1987. Units: mm/day.

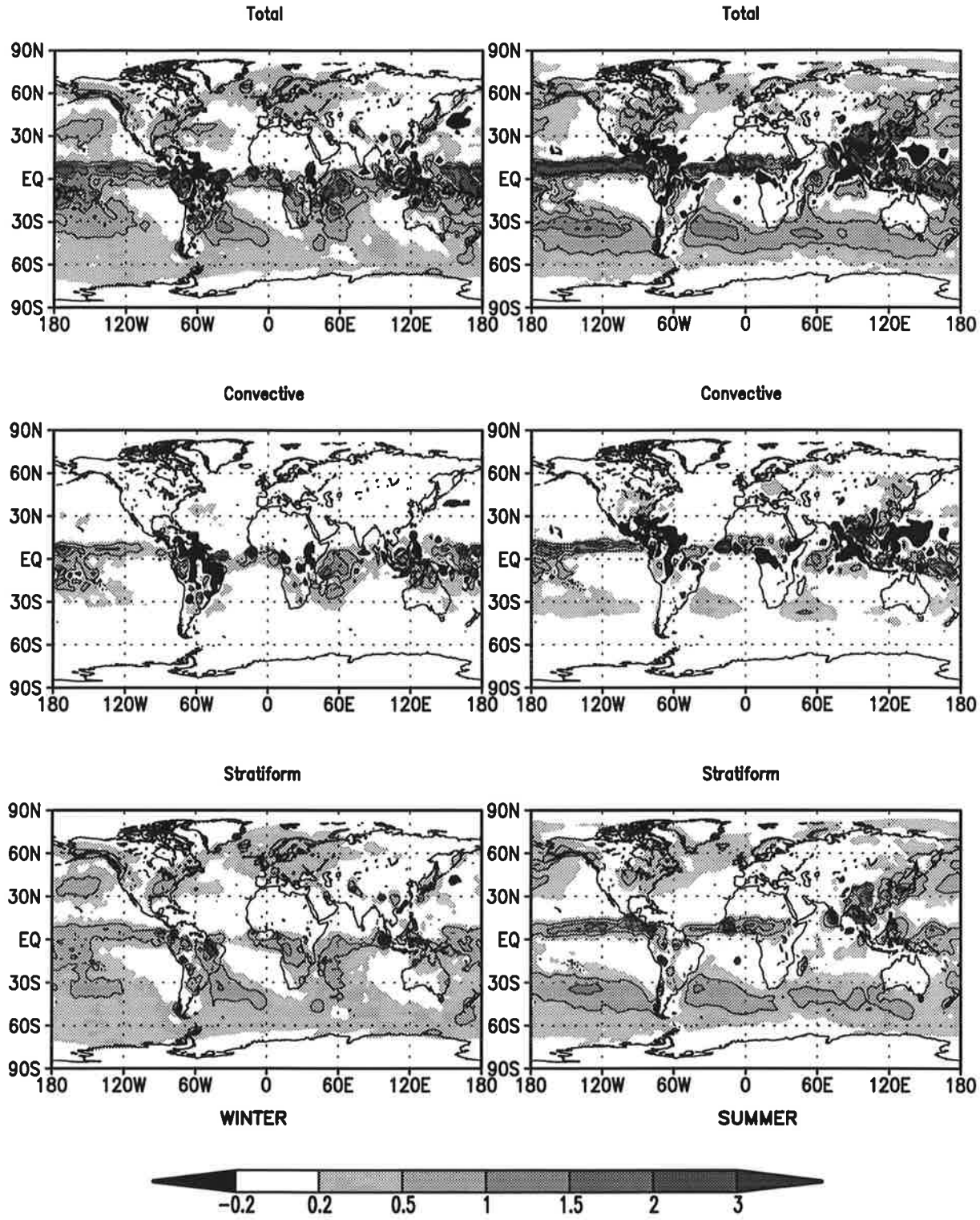

Fig. 13: Spinup in the ECMWF reanalysis. Left: winter (DJF 1979/80-1992/93), right: summer (JJA 1979-1993). Top: Total spinup, center: spinup of convective precipitation, bottom: spinup of stratiform precipitation. Units: mm/day. Contour interval 1 mm/day.

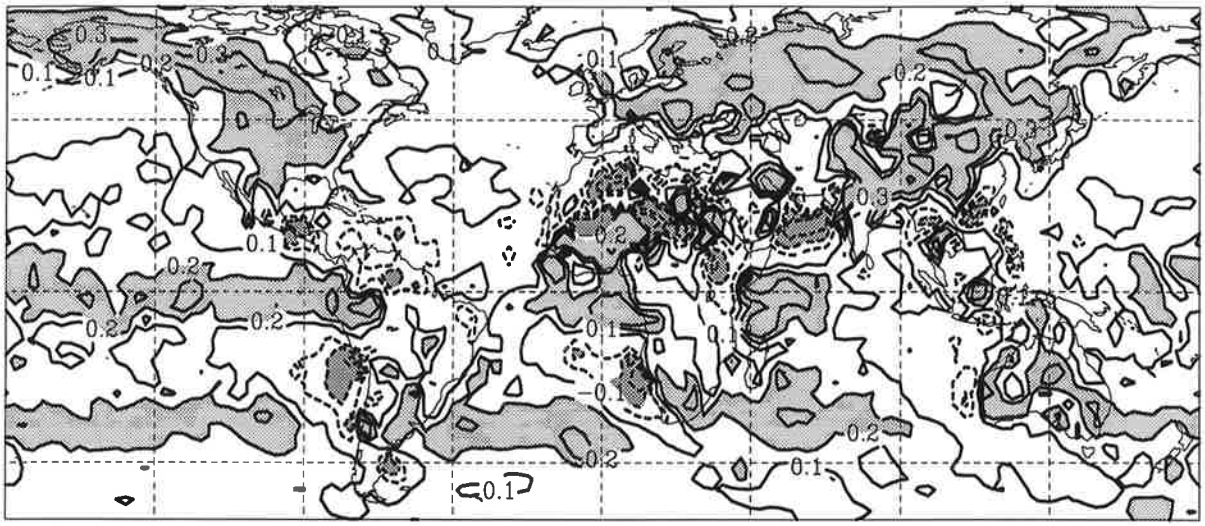

Fig. 14: Ratio of the spinup to the maximum of ERA06 and ERA24 for boreal winter (DJF 1979-1993). Contour interval 0.1, zero line is suppressed.

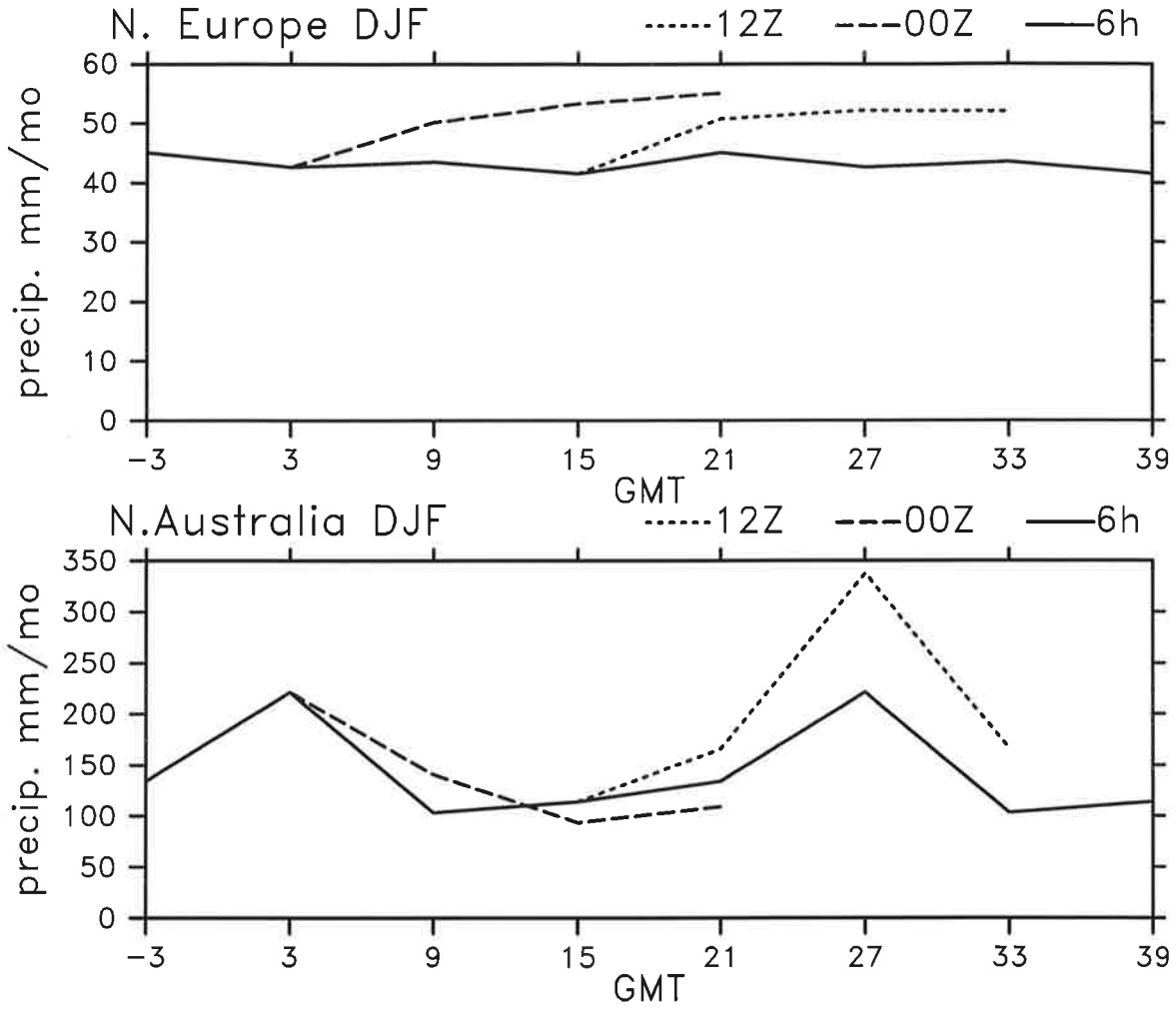

Fig. 15: Diurnal cycle of total spinup in winter (DJF 1979/80-1992/93) for Northern Europe (upper panel) and Northern Australia (lower panel). Units: mm/month.

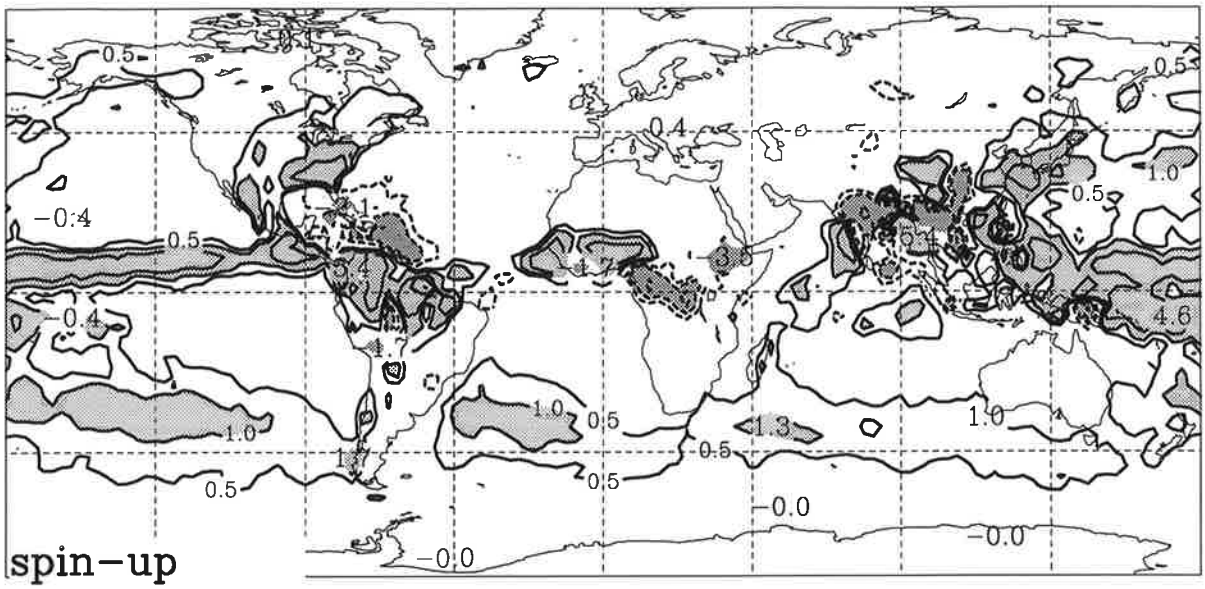

Fig. 16: Difference of the spinup in ERA forecasts started at 00 UTC minus forecasts started at 12 UTC for boreal summer (JJA 1979-1993). Units: mm/day, contour interval 1 mm/day, zero line is suppressed.

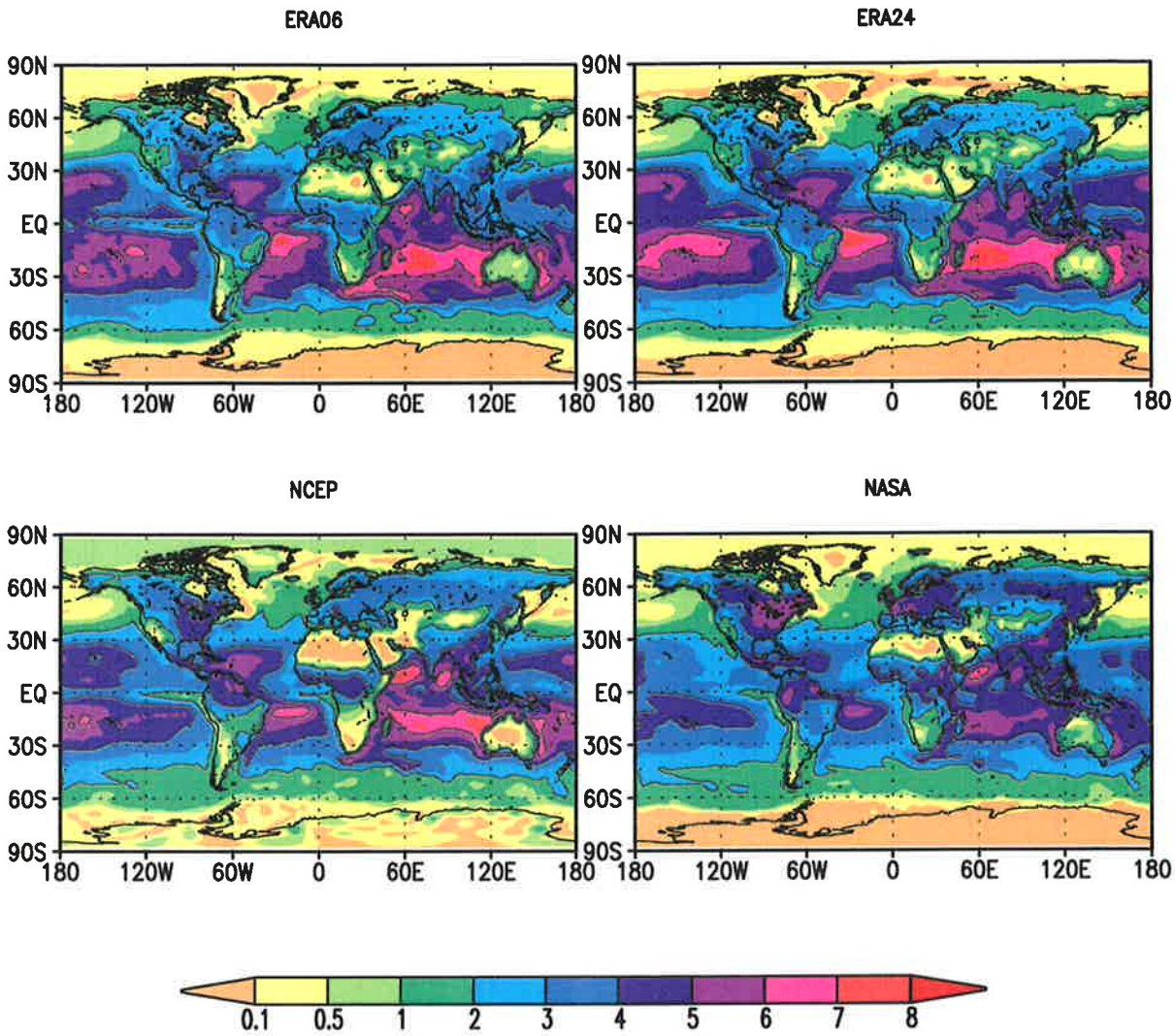

Fig. 17: Evaporation in summer (JJA 1988-1993). Top left: ECMWF reanalysis (ERA06), top right: ECMWF reanalysis (ERA24), bottom left: NCEP reanalysis, bottom right: NASA reanalysis. Units: mm/day. Contour interval: 2 mm/day.

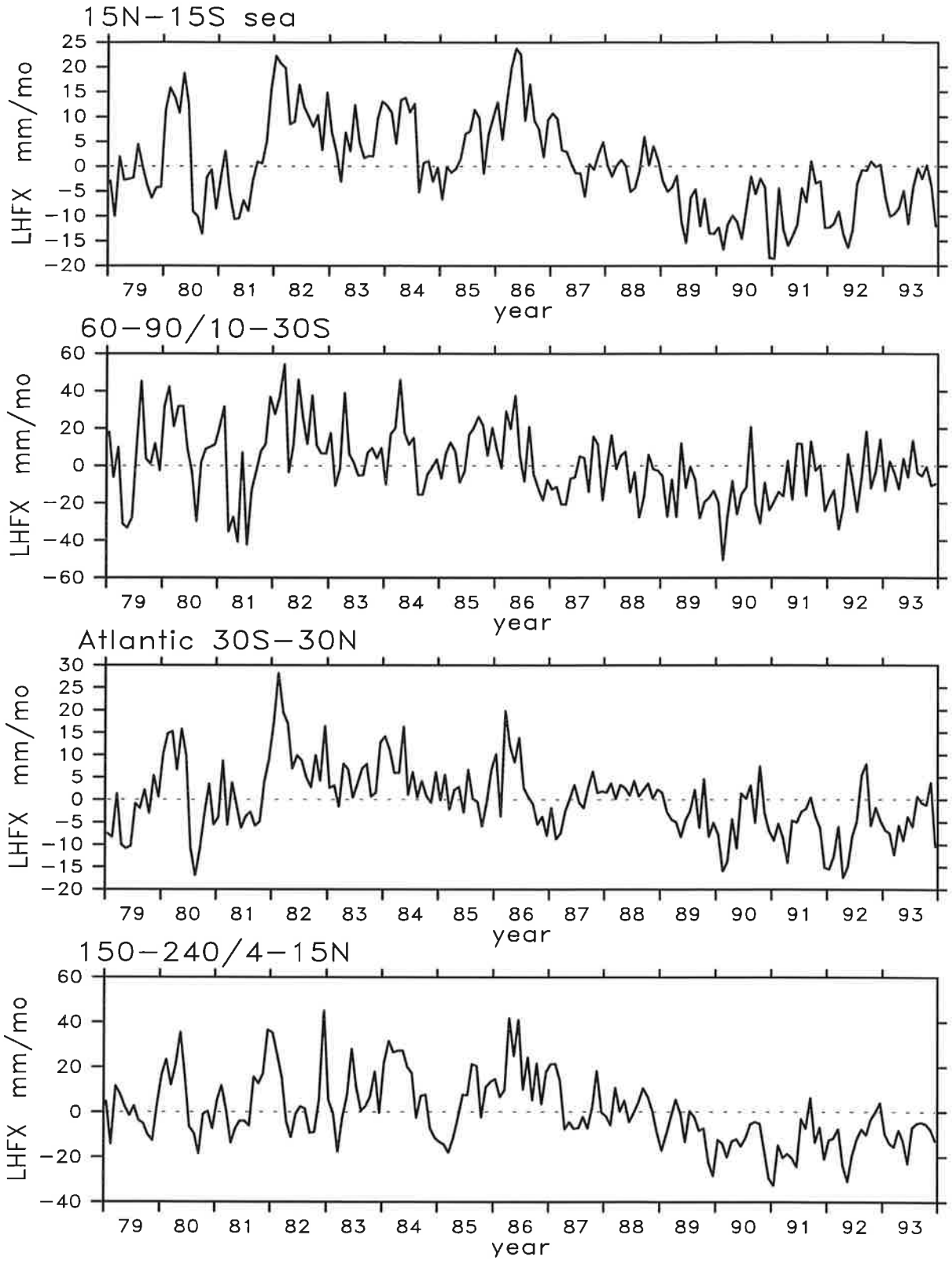

Fig. 18: Time series of latent heat flux deviation from mean 1979-1993 for all tropical oceans (top) and Indian Ocean, southern subtropical Atlantic and tropical Pacific, respectively (lower panels). Units: mm/month.

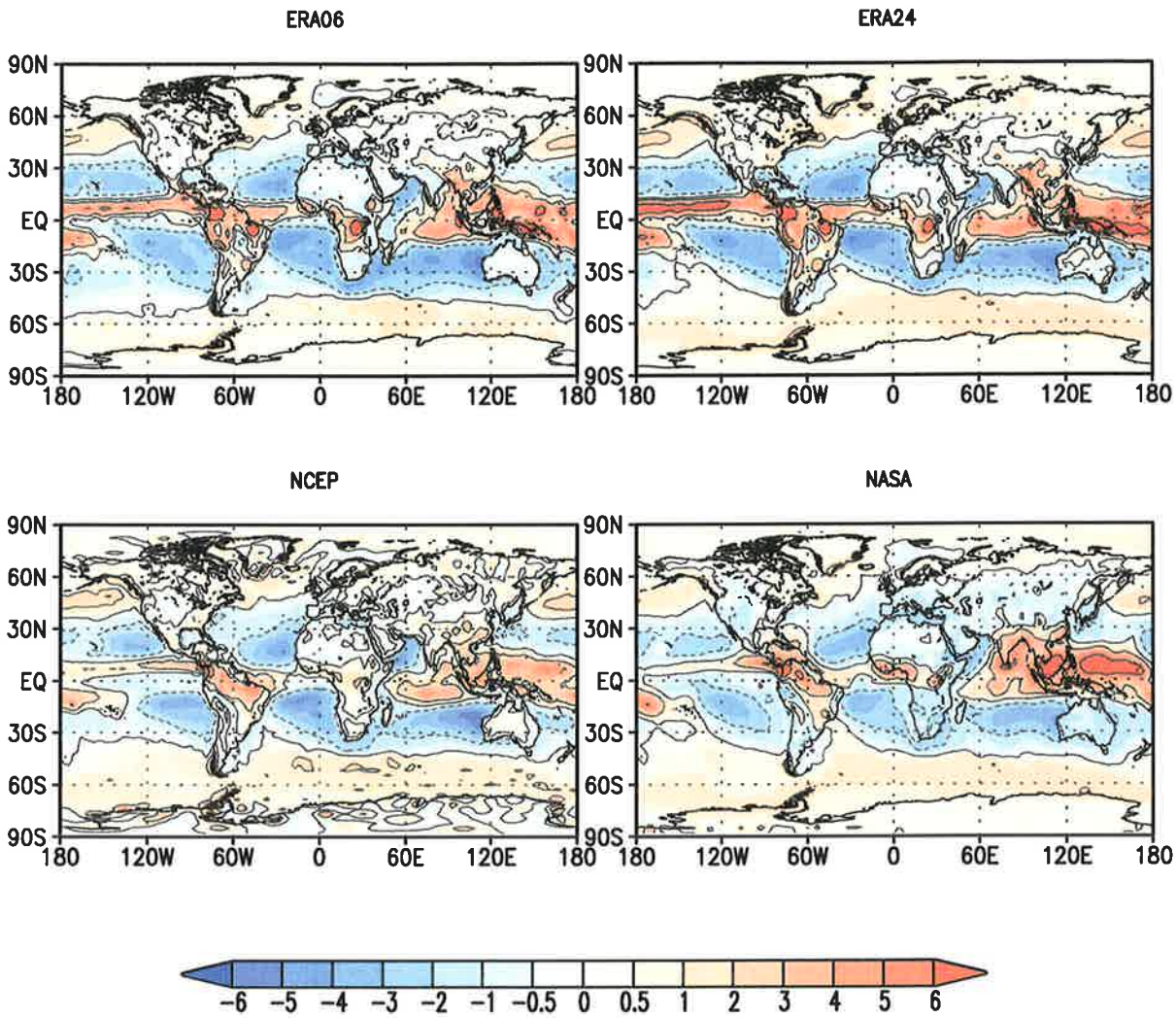

Fig. 19: Precipitation minus evaporation (P-E). Mean over the period 1988-1992. Top left: ECMWF reanalysis (ERA06), top right: ECMWF reanalysis (ERA24), bottom left: NCEP reanalysis, bottom right: NASA reanalysis. Units: mm/day. Contours at -2, 0, 2 and 6 mm/day.

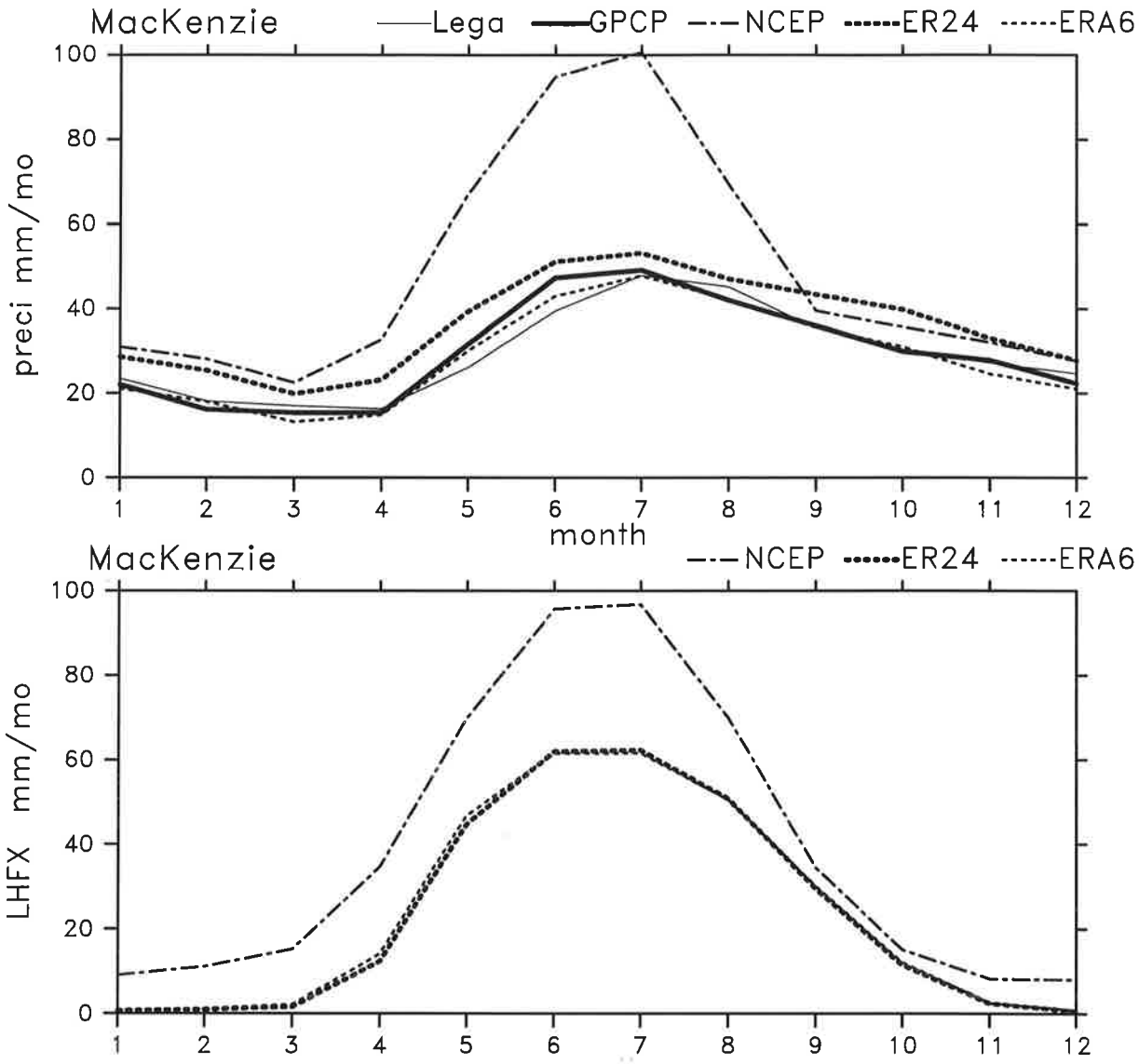

Fig. 20: Elements of the hydrological cycle in the Mackenzie river catchment. Top: precipitation, bottom: evaporation. ERA: mean for 1979-1993, NCEP: mean for 1982-1992, GPCP: mean for 1986-1994. Units: mm/month.